Energy Economics 151 (2025) 108809

Contents lists available at ScienceDirect

Energy Economics

journal homepage: www.elsevier.com/locate/eneco

Energy commodities and calendar spread options☆

Carme Frau [a,*], Gianluca Fusai [b,c], Ioannis Kyriakou [b]

[a] Departament d'Economia de l'Empresa, Universitat de les Illes Balears, Carretera de Valldemossa km. 7.5, 07122 Palma, Spain
[b] Bayes Business School, City St George's, University of London, 106 Bunhill Row, London EC1Y 8TZ, United Kingdom
[c] Dipartimento di Studi per l'Economia e l'Impresa, Università del Piemonte Orientale, Via Perrone 18, 28100 Novara, Italy

ARTICLE INFO

JEL classification:
C63
G13

Keywords:
Energy commodities
Bivariate models
Joint characteristic function
Estimation
Calendar spread option

ABSTRACT

We present a unified framework for pricing calendar spread options on energy commodities under affine models featuring stochastic volatility, jumps, and Samuelson effect. Expressions for the joint characteristic function of log-futures prices are derived, enabling efficient calibration and valuation. An empirical analysis, across WTI crude oil, HH natural gas, and ULSD heating oil shows that stochastic volatility models consistently outperform others. Jumps enhance short-term fit, while volatility dynamics matter more at longer maturities. The Black model remains competitive for short- and mid-term contracts.

1. Introduction

There are different types of spreads in the energy markets. These are usually based on price differences of the same commodity at different locations (location spreads) or at different times (calendar spreads), on differences in grades of the same commodity (quality spreads), or on differences between input and output prices (production spreads). Among the latter, relevant types include crack, fracking, and spark spreads. In this work, we focus on calendar spreads on futures contracts of energy commodities.

A calendar spread involves the simultaneous purchase and sale of contracts on the same commodity with different maturities. Calendar spread futures and options are typically used to profit from time decay (theta advantage), price volatility, or neutral price movements of the underlying asset. In terms of open interest, calendar spread options (CSOs) are the third most traded type of option in the energy markets, following European plain vanilla options (PVOs) and American options. As of September 14, 2023, open interest at NYMEX totaled 6.8 million contracts: CSOs accounted for 8.83% of this total, European PVOs 49.14%, American options 36.57%, and Asian options 3.22% (see Table 1 for a classification by energy type).

The objective of this paper is to develop a unified pricing framework for CSOs under a broad class of affine models, including those with stochastic volatility, jumps, and Samuelson effect. While Schneider and Tavin (2018) introduced a futures-based stochastic volatility model and computed the joint characteristic function (JCF) for pricing CSOs, their framework limits its direct applicability to other models. In contrast, we clearly separate these components and generalize the methodology to a wider class of affine models. Central to our approach is the derivation of closed-form expressions for the JCF of log-futures prices. This allows for efficient model calibration and CSO pricing across different specifications. In addition, we propose a novel approach that leverages conditioning arguments to price spread options under advanced stochastic volatility models, such as those where direct computation of the bivariate characteristic function is numerically demanding. This contributes to a unified and efficient framework for model calibration and CSO pricing.

Several authors have proposed approximation formulas for pricing spread options. Kirk (1995) was the first to offer an approximate solution, still widely used in practice, by generalizing the Margrabe (1978) exchange option formula for arbitrary strikes. Numerous extensions of Kirk's approach have followed. Bjerksund and Stlensland (2014) proposed a refined version that provides a very tight lower bound in a bivariate geometric Brownian motion model setting. Venkatramanan and Alexander (2011) expressed the spread option price as the sum of two compound options, deriving a new analytical approximation. Dempster and Hong (2002) pioneered the use of the two-dimensional fast Fourier transform (2D FFT) for

☆ This article is part of a Special issue entitled: 'Energy Finance and Energy Economics' published in Energy Economics.

* Corresponding author.
E-mail addresses: carme.frau@uib.es (C. Frau), gianluca.fusai.1@city.ac.uk, gianluca.fusai@uniupo.it (G. Fusai), ioannis.kyriakou@city.ac.uk (I. Kyriakou).

https://doi.org/10.1016/j.eneco.2025.108809
Received 2 July 2024; Received in revised form 31 July 2025; Accepted 3 August 2025
Available online 17 September 2025

Table 1
Open interest.
Source: CME Group.

Option type	No. contracts	Percentage (%)
Crude Oil	**3,130,512**	**46.28%**
Crude Oil (American)	2,366,500	34.98%
WTI Average Price	198,179	2.93%
WTI Crude Oil 1M Calendar Spread	167,750	2.48%
Crude Oil Financial 1M Calendar Spread	155,535	2.30%
WTI-Brent Crude Oil Spread	85,925	1.27%
Light Sweet Crude Oil European Financial	56,494	0.84%
Brent Last Day Financial European	29,297	0.43%
Micro WTI Crude Oil	17,542	0.26%
Natural Gas	**3,569,858**	**52.77%**
Natural Gas (European)	3,148,464	46.54%
Natural Gas (HH) Last-day Financial 1M Spread	156,253	2.31%
Natural Gas (HH) Last-day Financial 3M Spread	103,050	1.52%
Natural Gas (American)	88,254	1.30%
Natural Gas (HH) Last-day Financial	71,950	1.06%
Refined products	**57,474**	**0.85%**
NY Harbor ULSD Average Price	19,835	0.29%
NY Harbor ULSD	18,882	0.28%
NY Harbor ULSD 1M Calendar Spread	14,800	0.22%
Total	**6,764,434**	**100.00%**

Notes: In this table, we present the open interest in energy option contracts on NYMEX as of September 14, 2023. CSO contracts (highlighted in blue) account for 8.83% of the total. We list option contracts that represent at least 0.1% of the total open interest for each individual underlying.

pricing generic spread options. The method of Hurd and Zhou (2010) also requires evaluating a double integral numerically via the 2D FFT, and can become particularly cumbersome when applied to advanced bivariate models, such as those incorporating stochastic volatility and time-dampening price volatility (see later in Section 3). In contrast, Caldana and Fusai (2013) propose a fast and accurate one-dimensional Fourier inversion method. Their approach generalizes the lower-bound approximation of Bjerksund and Stlensland (2014) to any model for which the JCF of the logarithm of the prices in the spread is available in closed form.

Our empirical analysis, based on market data, focuses on three major energy benchmarks: WTI crude oil, Henry Hub natural gas, and ULSD heating oil. Each model is calibrated in two steps, first to PVOs on individual futures, then to CSO quotes to capture the correlation structure. The results show that stochastic volatility models, particularly Heston (1993) and Schneider and Tavin (2018), provide superior performance in fitting PVO prices. The inclusion of jumps enhances the fit at short maturities, while stochastic volatility becomes more critical at longer horizons. In terms of CSO pricing errors, the Heston (1993) model consistently delivers the lowest RMSE and minimal bias across contracts, with Schneider and Tavin (2018) performing comparably. By contrast, the Merton (1976) model performs weakest, especially for long-dated spreads. Notably, the Black (1976) model remains competitive for short- and mid-term contracts.

The remainder of this article is structured as follows. In Section 2, we introduce our methodology and present the construction of the JCF for CSO pricing. Section 3 details this for different models. In Section 4, we carry out an empirical analysis using market prices (futures, spreads, and CSOs) for three energy benchmarks: West Texas Intermediate (WTI) light sweet crude oil, Henry Hub (HH) natural gas, and New York Harbor ultra-low sulfur diesel (ULSD), a heating oil. Section 5 presents the option valuation results for our panel of models, and compares their accuracy. Section 6 concludes the paper and outlines avenues for future research.

2. Calendar spread options

Let $F(t,T)$ denote the futures price observed at time t with maturity at T, and let $f(t,T) \equiv \ln F(t,T)$ be the corresponding log-price. In Section 3, we consider models originally developed for spot prices and adapt them to model futures prices directly. This is motivated by the fact that, in most cases, commodities are quoted in terms of futures prices, as spot prices are not always available. Note that when $T = t$, the futures price with instantaneous maturity coincides with the spot price, that is, $F(t,t) \equiv S(t)$. Therefore, one can easily move from futures- to spot-based formulations, should spot price data be available.

This paper focuses on energy commodities. In particular, we analyze benchmarks for crude oil, natural gas, and heating oil. The futures term structure of each energy commodity reflects a combination of factors specific to its production, usage, and market dynamics. These include storage costs, supply and demand conditions, production estimates, seasonal patterns, geopolitical events, and infrastructure constraints. For example, crude oil prices are heavily influenced by production forecasts, natural gas exhibits pronounced seasonal effects, and heating oil is affected by both factors.

CSOs are written on the price difference between two futures contracts with different maturities. They offer a leveraged instrument for hedging or speculating on changes in the shape of the futures term structure.[1] CSOs are a variant of spread options, whose payoff depends on the difference between two underlying instruments. Such spreads can be constructed from contracts on different assets with the same maturity (intercommodity spreads) or from contracts on the same asset with different maturities (intracommodity spreads). The former includes varieties such as crack and spark spreads. CSOs correspond to the latter type, and this study focuses exclusively on them.

[1] Certain commodities can be stored, enabling their use in hedging strategies.

Table 2
Univariate future price dynamics.

Model	Dynamics	Volatility	Jumps
Bla76	$\frac{dF(t,T)}{F(t,T)} = \sigma_F dW_t^F$	σ_F constant	
Mer76	$\frac{dF(t,T)}{F(t,T)} = -\lambda \mathbb{E}_t^{\mathbb{Q}}\left[e^{J_F}-1\right]dt + \sigma_F dW_t^F + \left(e^{J_F}-1\right)dN_t$	σ_F constant	$J_F \sim \mathcal{N}(\mu_J, \sigma_J^2)$
Hes93	$\frac{dF(t,T)}{F(t,T)} = \sigma_F \sqrt{V_t} dW_t^F$	σ_F constant	
	$dV_t = \kappa\left(\theta - V_t\right)dt + \sigma_V \sqrt{V_t} dW_t^V$	σ_V constant	
Bat96	$\frac{dF(t,T)}{F(t,T)} = -\lambda \mathbb{E}_t^{\mathbb{Q}}\left[e^{J_F}-1\right]dt + \sigma_F \sqrt{V_t} dW_t^F + \left(e^{J_F}-1\right)dN_t$	σ_F constant	$J_F \sim \mathcal{N}(\mu_J, \sigma_J^2)$
	$dV_t = \kappa\left(\theta - V_t\right)dt + \sigma_V \sqrt{V_t} dW_t^V$	σ_V constant	
ST18	$\frac{dF(t,T)}{F(t,T)} = \sum_{i=1}^{n} \sigma_{F_i}(t,T)\sqrt{V_{i,t}} dW_t^{F_i}$	$\sigma_{F_i}(t,T) = \alpha_i e^{-\gamma_i (T-t)}$	
	$dV_{i,t} = \kappa_i\left(\theta_i - V_{i,t}\right)dt + \sigma_{V,i}\sqrt{V_{i,t}} dW_t^{V_i}$	σ_{V_i} constant	

Notes: This table presents the univariate factor dynamics, in addition to the stochastic volatility dynamics and the volatility functions, where applicable.

To formalize, let T_1 and T_2 denote the maturities of two futures contracts written on the same underlying asset. The calendar spread $s(t, T_1, T_2)$ at time t is defined as the difference in prices between the shorter and longer maturity contracts:

$$s(t, T_1, T_2) \equiv F(t, T_1) - F(t, T_2), \tag{2.1}$$

where t is the valuation date and T_0 is the option expiration date, with $0 \le t < T_0 < T_1 < T_2$.[2] The arbitrage-free price at time t of a European CSO with strike K is given by

$$p_{\text{CSO}}(t, T_0, T_1, T_2, K) = P(t, T_0)\, \mathbb{E}_{T_0}^{\mathbb{Q}}\left[\max\left(\varphi \cdot \left(s(T_0, T_1, T_2) - K\right), 0\right)\right], \tag{2.2}$$

where the expectation is taken under the risk-neutral measure $\mathbb{Q}$ conditional on information at time T_0, $P(t, T_0)$ denotes the price at time t of a zero-coupon bond maturing at T_0, and $\varphi = 1$ (respectively, $\varphi = -1$) corresponds to a call-type (put-type) option.

3. Calendar spread options price modeling

3.1. Models for futures price dynamics

We consider a pool of seven models from the literature. The underlying asset in each model is quoted in the form of a futures contract. The models included are as follows:

(i) Black (1976) (Bla76): a geometric Brownian motion.
(ii) Merton (1976) (Mer76): an extension of Bla76 incorporating independent and identically distributed (i.i.d.) jumps in prices.
(iii) Heston (1993) (Hes93): an extension of Bla76 with instantaneous stochastic variance.
(iv) Bates (1996) (Bat96): a combination of Mer76 and Hes93.
(v) Schneider and Tavin (2018) (ST18): an extension of Hes93 with time-dampening volatility function.

In addition to the futures price $F(t, T_j)$, $j = 1, 2$, V_t denotes the variance process, $W_t^{F_j}$ the Brownian motion associated with the futures price $F(t, T_j)$, W_t^v the Brownian motion associated with the variance, N_t a Poisson process, and J_F the jump size. Key parameters include the futures price volatility $\sigma_F > 0$, $\mathbb{E}[dW_t^{F_1} dW_t^{F_2}] = \rho\, dt$, $\rho \in [-1, 1]$, the variance mean-reversion speed $\kappa > 0$, the long-run variance level $\theta > 0$, the variance volatility $\sigma_V > 0$, the jump arrival intensity $\lambda > 0$, and the jump size distribution parameters $\mu_J \in \mathbb{R}$ and $\sigma_J \in \mathbb{R}_+$.

Our panel spans both Gaussian and non-Gaussian (log) dynamics, as well as uni-factor and multi-factor structures. In jump models, we assume only idiosyncratic (i.e., uncorrelated) jumps. We distinguish between models, whose univariate futures price dynamics are summarized in Table 2. In the bivariate case, the Group 1 models (Bla76, Mer76, Hes93, Bat96) have dynamics given in the general form by

$$\begin{aligned} \frac{dF(t,T_j)}{F(t,T_j)} &= \sigma_{F_j}\sqrt{V_t}\, dW_t^{F_j} - \lambda_j \mathbb{E}^{\mathbb{Q}}\left[e^{J_F}-1\right]dt + \left(e^{J_F}-1\right)dN_t, \quad j = 1, 2, \\ dV_t &= \kappa(\theta - V_t)dt + \sigma_V \sqrt{V_t}\, dW_t^V, \end{aligned} \tag{3.1}$$

with $\mathbb{E}[dW_t^{F_j} dW_t^V] = \rho_{FV}\, dt$, $\rho_{FV} \in [-1, 1]$, for both futures, $J_F \sim \mathcal{N}(\mu_J, \sigma_J^2)$, $F(0, T_1) \neq F(0, T_2) > 0$, and $V_0 > 0$. All Group 1 models share similar structural characteristics in their dynamics and exhibit a common form for the CF terms. Uni-factor models have i.i.d. increments (Bla76, Mer76), while multi-factor models incorporate stochastic volatility (Hes93, Bat96): for $dN_t \equiv 0$, we obtain Hes93; for $dV_t \equiv 0$, we recover Mer76, with additional $dN_t \equiv 0$ leading to Bla76. A second group of models generally includes those featuring time-dampening price volatility (see Trolle and Schwartz, 2009, Schneider and Tavin, 2018, Crosby and Frau, 2022). Our framework can accommodate all Group 2 models (more details can be

[2] For the CSO market, trading terminates on the business day prior to the termination of trading in the first leg of the underlying spread. The NYMEX (CME Group) contract specifications can be found here for 1M CSOs on WTI, here for 3M CSOs on HH, and here for 1M CSOs on ULSD.

Table 3
System of ODEs in bivariate models.

(a) ODE terms

Model	$\partial A(T_0-t;u_1,u_2)/\partial(T_0-t)$	$\partial C(T_0-t;u_1,u_2)/\partial(T_0-t)$
Bla76	b_0	0
Mer76	$b_0+\Lambda(u_1,u_2)$	0
Hes93	$\kappa\theta C(T_0-t;u_1,u_2)$	$b_0+b_1C(T_0-t;u_1,u_2)+b_2C^2(T_0-t;u_1,u_2)$
Bat96	$\kappa\theta C(T_0-t;u_1,u_2)+\Lambda(u_1,u_2)$	$b_0+b_1C(T_0-t;u_1,u_2)+b_2C^2(T_0-t;u_1,u_2)$
ST18	$\kappa\theta C(T_0-t;u_1,u_2)$	$b_0+b_1C(T_0-t;u_1,u_2)+b_2C^2(T_0-t;u_1,u_2)$

(b) ODE solutions

Model	$A(\tau;u_1,u_2)$	$C(\tau;u_1,u_2)$
Bla76	τb_0	0
Mer76	$\tau\left(b_0+\Lambda(u_1,u_2)\right)$	0
Hes93	$-\frac{\kappa\theta}{2b_2}\left((b_1+d)\tau+2\ln\frac{1-ge^{-d\tau}}{1-g}\right)$	$-\frac{b_1+d}{2b_2}\left(\frac{1-e^{d\tau}}{1-ge^{-d\tau}}\right)$
Bat96	$-\frac{\kappa\theta}{2b_2}\left((b_1+d)\tau+2\ln\frac{1-ge^{-d\tau}}{1-g}\right)+\tau\Lambda(u_1,u_2)$	$-\frac{b_1+d}{2b_2}\left(\frac{1-e^{d\tau}}{1-ge^{-d\tau}}\right)$
ST18	$\frac{\kappa\theta\gamma_i}{b_2}\left(\beta_i\tau-\frac{\mu_i z_i+\ln g(z_i)}{\gamma_i}+\frac{\mu_L}{\omega_i}\right)$	$\frac{\gamma_i}{b_2}\left(\beta_i+\mu_i z_i+z_i\frac{g'(z_i)}{g(z_i)}\right)$

(c) ODE parameters

Model	b_0	b_1	b_2
Bla76	$-\frac{1}{2}\left(\sum_{j=1}^{2}(u_j^2+iu_j)\cdot\sigma_{F_j}^2+2\rho\prod_{j=1}^{2}u_j\cdot\sigma_{F_j}\right)$	–	–
Mer76	$-\frac{1}{2}\left(\sum_{j=1}^{2}(u_j^2+iu_j)\cdot\sigma_{F_j}^2+2\rho\prod_{j=1}^{2}u_j\cdot\sigma_{F_j}\right)$	–	–
Hes93	$-\frac{1}{2}\left(\sum_{j=1}^{2}(u_j^2+iu_j)\cdot\sigma_{F_j}^2+2\rho\prod_{j=1}^{2}u_j\cdot\sigma_{F_j}\right)$	$-\kappa+\sigma_V\rho_{FV}\sum_{j=1}^{2}iu_j\cdot\sigma_{F_j}$	$\frac{1}{2}\sigma_V^2$
Bat96	$-\frac{1}{2}\left(\sum_{j=1}^{2}(u_j^2+iu_j)\cdot\sigma_{F_j}^2+2\rho\prod_{j=1}^{2}u_j\cdot\sigma_{F_j}\right)$	$-\kappa+\sigma_V\rho_{FV}\sum_{j=1}^{2}iu_j\cdot\sigma_{F_j}$	$\frac{1}{2}\sigma_V^2$
ST18	$-\frac{1}{2}\left(\sum_{j=1}^{2}(u_j^2+iu_j)\cdot\sigma_{F_j}^2(t,T_j)+2\rho\prod_{j=1}^{2}u_j\cdot\sigma_{F_j}(t,T_j)\right)$	$-\kappa+\sigma_V\rho_{FV}\sum_{j=1}^{2}iu_j\cdot\sigma_{F_j}(t,T_j)$	$\frac{1}{2}\sigma_V^2$

Notes: Panel (a) presents the ODE terms for the components of the characteristic exponent in the JCF defined in Eq. (3.6); Panel (b) presents the ODE solutions; and Panel (c) the associated ODE parameters. The jump-related term $\Lambda(u_1,u_2)$ is given in Eq. (A.4); the functions $g(z_i)$ and $g'(z_i)$ are defined in Eq. (A.8); z_i,β_i,μ_i for ST18 are specified in Eq. (A.10). For Hes93 and Bat96, we use $d=\sqrt{b_1^2-4b_0b_2}$ and $g=(b_1-d)/(b_1+d)$.

made available upon request), provided sufficient data are available. For illustration, we focus here on the ST18 model, whose bivariate dynamics are given by

$$\begin{aligned}\frac{dF(t,T_j)}{F(t,T_j)}&=\sigma_{F_j}(t,T_j)\sqrt{V_t}\,dW_t^{F_j},\quad j=1,2,\\ dV_t&=\kappa(\theta-V_t)dt+\sigma_V\sqrt{V_t}\,dW_t^{V}.\end{aligned}\tag{3.2}$$

These stochastic volatility models with time-dependent price volatility incorporate the Samuelson effect, that is, the volatility of futures prices increases as the contract approaches maturity. This occurs because short-dated futures prices are more sensitive to new information (e.g., shocks in supply and demand or spot prices) than long-dated ones. The precise model depends on the functional form of $\sigma_{F_j}(t,T_j)$: for example, for ST18, $\sigma_{F_j}(t,T_j)=\alpha_j\exp(-\gamma_j(T_j-t))$, where $\alpha_1\neq\alpha_2,\alpha_1,\alpha_2>0$, and $\gamma_1\neq\gamma_2,\gamma_1,\gamma_2>0$. It is worth noting that ST18 reduces to Hes93 as $\gamma\to 0$. Throughout, we assume a common variance process V_t across both futures in the spread.

3.2. Characteristic function approach

Recent literature has proposed several efficient methods for pricing spread options, with particular emphasis on Fourier-based techniques. Among them, Caldana and Fusai (2013) and Bjerksund and Stlensland (2014) present a pricing formula in the form of a lower bound. As discussed in Schneider and Tavin (2018), this lower bound is shown to be extremely tight and is often regarded as the option price itself.[3] An alternative method is introduced in Hurd and Zhou (2010), which involves pricing spread options via a two-dimensional Fourier inversion using, nevertheless, complex gamma functions. Alfeus and Schloegl (2019) carries out a detailed empirical study of bivariate models, including those of Black and Scholes (1973) and Heston (1993), and evaluates the performance of the Hurd and Zhou (2010) method by comparing it with Monte Carlo simulation and the lower-bound approach of Caldana and Fusai (2013). Their findings show that Caldana and Fusai (2013) consistently delivers reliable results across the different model specifications. Given the demonstrated accuracy and efficiency of the lower-bound approach proposed by Caldana and Fusai (2013), which provides a robust and computationally tractable alternative to more complex inversion techniques, especially for advanced bivariate models (see Section 3), it stands out as a particularly appealing method for practical implementation. Its ability to accommodate a broad class of non-Gaussian processes, while circumventing the need for two-dimensional Fourier inversion, further reinforces its suitability for empirical work. Besides, given the practical reality that model parameters are never known exactly, the use of an approximating technique (here a bound), especially one that is highly accurate, does not constitute an actual limitation of the methodology.

[3] In fact, when the strike $K=0$, the lower bound becomes exact and can be seen as a generalization of the traditional Margrabe formula in non-Gaussian model settings.

To this end, let us first define the vectors $\mathbf{u} \equiv (u_1, u_2) \in \mathbb{R}^2$, $\mathbf{T} \equiv (T_1, T_2)$, and $\mathbf{F} \equiv \mathbf{F}(T_0, \mathbf{T}) \equiv \left(F(T_0, T_1), F(T_0, T_2)\right)^\top$. We consider the transform involving the two futures prices forming the spread $s(t, T_1, T_2)$, as defined in Eq. (2.1), which is given by

$$\Phi_{\mathbf{F}}(\mathbf{u}) \equiv \mathbb{E}_t^{\mathbb{Q}}\left[e^{i\mathbf{u}\cdot\ln\mathbf{F}(T_0,\mathbf{T})}\right] = \mathbb{E}_t^{\mathbb{Q}}\left[e^{iu_1\ln F(T_0,T_1)+iu_2\ln F(T_0,T_2)}\right]. \tag{3.3}$$

Following Caldana and Fusai (2013), the lower bound for the time-t price of a CSO call is given by

$$LB_{\text{CSO}}(t, T_0, T_1, T_2, K) = \frac{P(t,T_0)}{\pi}\, e^{-\delta k} \int_0^\infty e^{-iuk}\Psi_{\mathbf{F}}(u)\, du, \tag{3.4}$$

where

$$\begin{aligned} \Psi_{\mathbf{F}}(u) &= \frac{e^{i\eta\ln\Phi_{\mathbf{F}}(0,-i\alpha)}}{i\eta}\left(\Phi_{\mathbf{F}}(\eta - i, -\alpha\eta) - \Phi_{\mathbf{F}}(\eta, -\alpha\eta - i) - K\Phi_{\mathbf{F}}(\eta, -\alpha\eta)\right), \\ k &= \ln\left(F(t,T_2) + K\right), \qquad \eta = u - i\delta, \qquad \alpha = \frac{F(t,T_2)}{F(t,T_2)+K}, \end{aligned} \tag{3.5}$$

and δ is a damping parameter that introduces exponential decay in the integrand to ensure integrability in the Fourier space. Obviously, to evaluate the CSO price, one must define the JCF in Eq. (3.3) according to the chosen model. For all models considered in this paper, the JCF admits an exponential-affine form, with its structure governed by the dynamics of the underlying risk factors. The functions appearing in the characteristic exponent are solutions to Riccati differential equations. Notably, under i.i.d. increments, the JCF simplifies considerably.

Proposition 1. *Assuming a general affine process with stochastic volatility and jumps, the JCF of the logarithm of the futures prices in spread (2.1), $f(T_0, T_j) = \ln F(T_0, T_j)$, $j = 1, 2$, is given by*

$$\mathbb{E}_t^{\mathbb{Q}}\left[e^{iu_1 f(T_0,T_1)+iu_2 f(T_0,T_2)}\right] = \exp\left\{iu_1 f(t,T_1) + iu_2 f(t,T_2) + A(T_0 - t; u_1, u_2) + C(T_0 - t; u_1, u_2)V_t\right\}. \tag{3.6}$$

The functions $A(T_0 - t; u_1, u_2)$ and $C(T_0 - t; u_1, u_2)$ are provided in Table 3b.

Proof. The proof relies on the affine structure of a model. More details are provided in Appendix A. The solutions for terms A and C of the different models' ordinary differential equations (ODEs) are summarized in Table 3b. For models without stochastic volatility, the C term vanishes. ■

3.3. Conditional Monte Carlo approach

In general, transform techniques relying on characteristic functions may exhibit slowness and numerical inaccuracy when the evaluation involves special functions, as is the case with the ST18 model. In such settings, a reliable alternative is Monte Carlo simulation, which circumvents these challenges.

For the ST18 model, this approach is particularly effective since the log-futures prices are jointly normal conditional on a path of the Brownian motion driving the variance process. This permits the use of conditional Monte Carlo simulation, namely, the outer (unconditional) pricing expectation requires evaluating an inner (conditional) expectation across a number of variance sample paths.[4] Consequently, the inner expectation can be evaluated either via the conditional-normality-based lower-bound method, which benefits from a simpler joint characteristic function, or via Ravindran (1993)'s exact expression. While the latter is theoretically exact, its implementation requires numerical integration, which can be computationally demanding. Therefore, from a practical standpoint, the lower-bound method retains an attractive balance between accuracy and computational efficiency.

Key to the conditional Monte Carlo approach are the conditioning arguments specific to ST18, which we detail in Proposition 2.

Proposition 2. *In the ST18 model, $f\left(T_0, T_j\right)$ has a conditional normal distribution, with mean*

$$f\left(t,T_j\right) - \frac{\alpha_j\rho_{FV}\kappa\theta}{\sigma_V\gamma_j}e^{-\gamma_j T_j}\left(e^{\gamma_j T_0} - e^{\gamma_j t}\right) + \frac{\alpha_j\rho_{FV}}{\sigma_V}e^{-\gamma_j T_j}\left(e^{\gamma_j T_0}V_{T_0} - e^{\gamma_j t}V_t\right) - \frac{\alpha_j^2}{2}\int_t^{T_0}\left(e^{-2\gamma_j(T_j-s)} - \frac{2\rho_{FV}\kappa}{\alpha_j\sigma_V}e^{-\gamma_j(T_j-s)} + \frac{2\rho_{FV}\gamma_j}{\alpha_j\sigma_V}e^{-\gamma_j(T_j-s)}\right)V_s\, ds.$$

The conditional covariance between the log-prices of futures for delivery at times T_i and T_j is given by

$$\alpha_i\alpha_j\rho\left(1-\rho_{FV}^2\right)\int_t^{T_0} e^{-\gamma_i(T_i-s)}e^{-\gamma_j(T_j-s)}V_s\, ds.$$

(For $T_i = T_j$, $\rho = 1$ and we obtain the variance.)

Proof. See Appendix B. ■

Remark 3. As $\gamma_i, \gamma_j \to 0$, ST18 reduces to Hes93, and the conditional mean and covariance simplify accordingly as

$$f\left(t,T_j\right) - \frac{\alpha_j\kappa\theta\rho_{FV}(T_0-t)}{\sigma_V} + \frac{\alpha_j\rho_{FV}}{\sigma_V}(V_{T_0} - V_t) - \frac{1}{2}\alpha_j^2\left(1 - \frac{2\rho_{FV}\kappa}{\alpha_j\sigma_V}\right)\int_t^{T_0} V_s\, ds,$$

and

$$\alpha_i\alpha_j\rho\left(1-\rho_{FV}^2\right)\int_t^{T_0} V_s\, ds.$$

[4] To this end, and similarly to Kyriakou et al. (2016a) and Kyriakou et al. (2016b), the method of Andersen (2008), based on central discretization, can also be adapted to ST18, while for Hes93 readers may alternatively find useful the approach proposed by Kyriakou et al. (2024).

Table 4
Market data — futures and spreads.

(a) WTI

Contract		Spr.1	Spr.2	Spr.3	Spr.4	Spr.5	Spr.6	Spr.7	Spr.8	Spr.9	Spr.10
F1	RIC	CLH3	CLJ3	CLK3	CLM3	CLN3	CLQ3	CLU3	CLV3	CLX3	CLZ3
	Mty.	21/02/23	21/03/23	20/04/23	22/05/23	20/06/23	20/07/23	22/08/23	20/09/23	20/10/23	20/11/23
	Del.	03/23	04/23	05/23	06/23	07/23	08/23	09/23	10/23	11/23	12/23
	Val.	78.47	78.69	78.84	78.81	78.56	78.18	77.71	77.21	76.70	76.21
F2	RIC	CLJ3	CLK3	CLM3	CLN3	CLQ3	CLU3	CLV3	CLX3	CLZ3	CLF24
	Mty.	21/03/23	20/04/23	22/05/23	20/06/23	20/07/23	22/08/23	20/09/23	20/10/23	20/11/23	19/12/24
	Del.	04/23	05/23	06/23	07/23	08/23	09/23	10/23	11/23	12/23	01/24
	Val.	78.69	78.84	78.81	78.56	78.18	77.71	77.21	76.70	76.21	75.71
Spr.	RIC	CLH3-J3	CLJ3-K3	CLK3-M3	CLM3-N3	CLN3-Q3	CLQ3-U3	CLU3-V3	CLV3-X3	CLX3-Z3	CLZ3-F24
	Mty.	21/02/23	21/03/23	20/04/23	22/05/23	20/06/23	20/07/23	22/08/23	20/09/23	20/10/23	20/11/23
	Del.	03/23	04/23	05/23	06/23	07/23	08/23	09/23	10/23	11/23	12/23
	Val.	−0.22	−0.15	0.03	0.25	0.38	0.47	0.50	0.51	0.49	0.50

(b) HH

Contract		Spr.1	Spr.2	Spr.3	Spr.4	Spr.5	Spr.6	Spr.7	Spr.8	Spr.9	Spr.10
F1	RIC	NGH3	NGJ3	NGK3	NGM3	NGN3	NGQ3	NGU3	NGV3	NGX3	NGZ3
	Mty.	24/02/23	29/03/23	26/04/23	26/05/23	28/06/23	27/07/23	29/08/23	27/09/23	27/10/23	28/11/23
	Del.	03/23	04/23	05/23	06/23	07/23	08/23	09/23	10/23	11/23	12/23
	Val.	2.396	2.477	2.646	2.840	3.017	3.075	3.044	3.122	3.546	3.944
F4	RIC	NGM3	NGN3	NGQ3	NGU3	NGV3	NGX3	NGZ3	NGF24	NGG4	NGH4
	Mty.	26/05/23	28/06/23	27/07/23	29/08/23	27/09/23	27/10/23	28/11/23	27/12/23	29/01/24	27/02/24
	Del.	06/23	07/23	08/23	09/23	10/23	11/23	12/23	01/24	02/24	03/24
	Val.	2.840	3.017	3.075	3.044	3.122	3.546	3.944	4.183	4.057	3.654
Spr.	RIC	NGH3-M3	NGJ3-N3	NGK3-Q3	NGM3-U3	NGN3-V3	NGQ3-X3	NGU3-Z3	NGV3-F4	NGX3-G4	NGZ3-H4
	Mty.	24/02/23	29/03/23	26/04/23	26/05/23	28/06/23	27/07/23	29/08/23	27/09/23	27/10/23	28/11/23
	Del.	03/23	04/23	05/23	06/23	07/23	08/23	09/23	10/23	11/23	12/23
	Val.	−0.444	−0.540	−0.429	−0.204	−0.105	−0.471	−0.900	−1.061	−0.511	0.290

(c) ULSD

Contract		Spr.1	Spr.2	Spr.3	Spr.4	Spr.5	Spr.6	Spr.7	Spr.8	Spr.9	Spr.10
F1	RIC	HOH3	HOJ3	HOK3	HOM3	HON3	HOQ3	HOU3	HOV3	HOX3	HOZ3
	Mty.	28/02/23	31/03/23	28/04/23	31/05/23	30/06/23	31/07/23	31/08/23	29/09/23	31/10/23	30/11/23
	Del.	03/23	04/23	05/23	06/23	07/23	08/23	09/23	10/23	11/23	12/23
	Val.	2.8933	2.8576	2.7997	2.7585	2.7403	2.7302	2.7273	2.7232	2.7164	2.7064
F2	RIC	HOJ3	HOK3	HOM3	HON3	HOQ3	HOU3	HOV3	HOX3	HOZ3	HOF24
	Mty.	31/03/23	28/04/23	31/05/23	30/06/23	31/07/23	31/08/23	29/09/23	31/10/23	30/11/23	29/12/24
	Del.	04/23	05/23	06/23	07/23	08/23	09/23	10/23	11/23	12/23	01/24
	Val.	2.8576	2.7997	2.7585	2.7403	2.7302	2.7273	2.7232	2.7164	2.7064	2.6982
Spr.	RIC	HOH3-J3	HOJ3-K3	HOK3-M3	HOM3-N3	HON3-Q3	HOQ3-U3	HOU3-V3	HOV3-X3	HOX3-Z3	HOZ3-F24
	Mty.	28/02/23	31/03/23	28/04/23	31/05/23	30/06/23	31/07/23	31/08/23	29/09/23	31/10/23	30/11/23
	Del.	03/23	04/23	05/23	06/23	07/23	08/23	09/23	10/23	11/23	12/23
	Val.	0.0357	0.0579	0.0412	0.0182	0.0101	0.0029	0.0041	0.0068	0.0100	0.0082

Notes: In this table, we report the futures prices and their spreads quoted on February 8, 2023. For WTI and ULSD, we consider 1M spreads, while for HH we consider 3M spreads. WTI prices are quoted in USD/barrel, HH prices in USD/MMBtu, and ULSD prices in USD/gallon. Spreads associated with the quoted CSOs listed in Table 6 are indicated in gray. Abbreviations: RIC (Reuters Instrument Code), Mty. (Maturity), Del. (Delivery month), Val. (Value).

4. Empirical investigation and model calibration

In this section, we present our empirical experiment. We begin by describing the dataset and proceed to outline the procedure used for the calibration exercise.

4.1. Market data

We begin by describing the market data used to calibrate the models. The dataset consists of futures prices and their corresponding PVOs, spreads on futures and the corresponding CSOs, all written on three energy benchmarks: WTI light sweet crude oil, HH natural gas, and ULSD heating oil. These contracts are listed on NYMEX and quoted in USD.[5] We use official market data from the Exchange as of February 8, 2023. It is worth noting that, although CSOs are listed also on other energy benchmarks (e.g., Chicago ethanol Platts, European low sulfur gasoil, RBOB gasoline), we have excluded due to zero traded volume on the observation date.

Each underlying commodity has its own conventions for trading months and maturity dates, which are detailed later. Contracts are identified by their delivery month, which follows the maturity month.[6] We adopt the industry convention of naming contracts using the delivery month letter followed by the final digit of the year. For example, H3 refers to a contract delivered in March 2023 (maturing in February 2023).

4.1.1. Crude oil

Our first dataset consists of 1M futures spreads and the corresponding 1M CSOs written on WTI crude oil. Futures prices and spreads are listed in Table 4a, PVO prices in Table 5a, and CSO prices in Table 6a. We include 10 one-month spread contracts, labeled Spr.i, where i refers to the ith 1M spread contract available: CLH3–J3 (Spr.1) to CLZ3–F24 (Spr.10) Each spread features up to seven moneyness levels. The dataset comprises

[5] Prices are quoted in: USD per barrel for WTI, USD per MMBtu (million British thermal units) for HH, and USD per gallon for ULSD.
[6] Delivery months are denoted by letters: F (Jan), G (Feb), H (Mar), J (Apr), K (May), M (Jun), N (Jul), Q (Aug), U (Sep), V (Oct), X (Nov), Z (Dec).

Table 5
Market data — PVO prices.

(a) WTI

Type	K	F1	F2	F3	F4	F5	F6	F7	F8	F9	F10	F11	ITM	OTM	Total
Put	70.0	0.08	0.96	1.93	2.89	3.68	4.49	5.24	5.86	6.50	7.05	7.57	–	11	11
	70.5	0.10	1.05	2.06	3.04	3.84	4.66	5.43	–	–	7.26	–	–	8	8
	71.0	0.11	1.14	2.19	3.20	4.01	4.84	5.62	6.26	–	7.47	–	–	9	9
	71.5	0.13	1.25	2.33	3.36	4.18	5.03	5.81	–	–	7.68	–	–	8	8
	72.0	0.16	1.36	2.48	3.52	4.36	5.22	6.01	–	–	7.90	–	–	8	8
Call	80.0	0.95	3.13	4.63	5.81	6.52	7.11	7.55	7.82	8.06	8.23	8.31	–	11	11
	80.5	0.78	2.91	4.40	5.58	6.30	6.89	7.34	–	7.85	8.02	–	–	9	9
	81.0	0.64	2.70	4.18	5.36	6.08	6.68	7.13	7.40	–	7.89	–	–	9	9
	81.5	0.52	2.50	3.97	5.15	5.86	6.47	6.92	–	–	7.63	–	–	8	8
	82.0	0.43	2.31	3.76	4.94	5.66	6.26	6.72	–	–	7.43	–	–	8	8
ITM	–	–	–	–	–	–	–	–	–	–	–	–			
OTM		10	10	10	10	10	10	10	4	3	10	2		89	
Total		10	10	10	10	10	10	10	4	3	10	2			89

(b) HH

Type	K	F1	F2	F3	F4	F5	F6	F7	F8	F9	F10	F11	ITM	OTM	Total
Put	2.30	–	–	–	–	–	–	–	0.2483	–	–	0.1042	–	2	2
	2.35	–	–	–	–	–	–	–	0.2627	–	–	–	–	1	1
	2.36	–	–	–	–	–	–	–	0.2656	–	–	–	–	1	1
	2.40	–	–	–	–	–	–	–	0.2777	–	–	0.1232	–	2	2
	2.44	–	–	–	–	–	–	–	0.2903	–	–	–	–	1	1
Call	4.30	–	–	–	–	–	–	–	0.1918	–	–	–	–	1	1
	4.35	–	–	–	–	–	–	–	–	–	–	0.7943	–	1	1
	4.42	–	–	–	–	–	–	–	–	–	–	0.7724	–	1	1
	4.50	–	–	–	–	–	–	–	0.1591	–	–	0.7485	–	2	2
	4.55	–	–	–	–	–	–	–	0.1520	–	–	–	–	1	1
ITM	–	–	–	–	–	–	–	–	–	–	–	–			
OTM	–	–	–	–	–	–	–	–	8	–	–	5	–	13	–
Total	–	–	–	–	–	–	–	–	8	–	–	5			13

(c) ULSD

Type	K	F1	F2	F3	F4	F5	F6	F7	F8	F9	F10	F11	ITM	OTM	Total
Put	2.40	0.0013	0.0180	0.0426	–	–	–	–	–	–	–	–	–	3	3
	2.41	–	–	0.0446	–	–	–	–	–	–	–	–	–	1	1
	2.42	–	–	0.0467	–	–	–	–	–	–	–	–	–	1	1
	2.43	0.0019	–	–	–	–	–	–	–	–	–	–	–	1	1
	2.49	–	0.0298	–	–	–	–	–	–	–	–	–	–	1	1
Call	2.90	0.0911	0.1413	–	–	–	–	–	–	–	–	–	–	2	2
	2.91	–	–	0.1545	–	–	–	–	–	–	–	–	–	1	1
	2.92	0.0825	0.1337	–	–	–	–	–	–	–	–	–	–	2	2
	2.93	0.0784	0.1300	0.1478	–	–	–	–	–	–	–	–	–	3	3
	2.94	0.0746	–	–	–	–	–	–	–	–	–	–	–	1	1
ITM		–	–	–	–	–	–	–	–	–	–	–			
OTM	–	6	5	5	–	–	–	–	–	–	–	–		16	–
Total		6	5	5	–	–	–	–	–	–	–	–			16

NOTES: In this table, we present quoted (ITM excluded) PVO prices associated with the underlyings in Table 4. For WTI, PVO prices are available for 11 contracts (8 of which have prices for all strikes), while for HH, prices are available for only 2 contracts, and for HO, for only 3 contracts.

91 options: 45 puts (49.45%) and 46 calls (50.55%), of which 75 (82.42%) are at-the-money (ATM) or out-of-the-money (OTM), and 16 (17.58%) are in-the-money (ITM) which we exclude from our analysis.

Trading months include all consecutive months for the current year and the next five years, plus June and December contracts extending beyond six years. The last trading day is three business days before the 25th calendar day of the month preceding the delivery month. The minimum price change is 0.01 USD per barrel.

4.1.2. Natural gas

The natural gas CSO market is highly concentrated, with liquidity primarily in two spread contracts: i) a 1M spread covering March–April (transition from winter to summer), and (ii) a 3M spread covering October–January (transition from summer to winter). In practice, no options are traded for other months. Our dataset includes only the 3M futures spreads on HH natural gas and the corresponding 3M CSOs, as there are no trades on the 1M spread. Futures prices and spreads are listed in Table 4b, PVO prices in Table 5b, and CSO prices in Table 6b. The only quoted spread contract is NGV3–F4 (Spr.8), for which we have eight options: four calls and four puts, seven of which are OTM.

Trading months include the current year and the next 12 years. A new calendar year is added upon expiry of the December contract. The last trading day is three business days before the first calendar day of the delivery month. The minimum price change is 0.001 USD per MMBtu.

4.1.3. Heating oil

Our third dataset consists of 1M futures spreads and the corresponding 1M CSOs written on ULSD. Futures prices and spreads are reported in Table 4c, PVO prices in Table 5c, and CSO prices in Table 6c. Only two 1M spread contracts are quoted in the market: HOH3–J3 and HOJ3–K3. The dataset includes 16 options: eight calls and eight puts, eight of which are OTM.

Trading months extend through the current year plus three additional years and one month. A new calendar year is added after the expiration of the December contract. Trading ends at the close of business on the last business day of the month preceding the delivery month.

Table 6
Market data — CSO prices.

(a) WTI

Type	K	Spr.1	Spr.2	Spr.3	Spr.4	Spr.5	Spr.6	Spr.7	Spr.8	Spr.9	Spr.10	ITM	OTM	Total
Put	−0.50	0.01	0.03	0.05	0.07	0.04	0.06	0.02	0.04	0.04	0.04	–	10	10
	−0.40	–	0.04	0.06	0.08	–	–	–	–	–	–	–	3	3
	−0.30	–	0.06	–	–	–	–	–	–	–	–	–	1	1
	−0.25	0.05	0.08	0.09	0.11	0.07	0.10	0.05	0.08	0.07	0.08	–	10	10
	0.00	0.25	0.25	0.19	0.17	0.15	0.17	0.12	0.15	0.15	0.16	2	8	10
	0.50	0.73	–	–	–	–	–	–	–	–	–	1	–	1
	0.75	0.97	0.92	0.77	0.63	0.64	0.57	0.57	0.57	0.60	0.59	10	–	10
Call	0.00	0.04	0.11	–	–	–	–	–	–	–	–	–	2	2
	0.25	–	0.07	–	–	–	–	–	–	–	–	–	1	1
	0.30	–	–	0.12	0.23	0.38	0.46	–	–	–	–	2	2	4
	0.50	0.01	0.04	0.09	0.18	0.33	0.37	0.39	0.41	0.42	0.42	1	9	10
	0.75	–	–	–	–	0.28	0.30	0.32	–	0.35	0.35	–	5	5
	1.00	–	–	–	0.10	0.23	0.24	0.27	0.28	0.30	0.29	–	7	7
	1.25	0.01	–	–	–	–	–	–	–	0.25	0.24	–	3	3
	1.50	0.01	–	–	–	0.15	0.16	0.18	0.20	0.22	0.21	–	7	7
	2.00	0.01	–	–	–	0.09	0.11	0.11	0.14	0.16	0.14	–	7	7
ITM		3	2	1	1	2	2	1	2	1	1	16		
OTM		7	7	6	7	8	8	8	6	9	9		75	
Total		10	9	7	8	10	10	9	8	10	10			91

(b) HH

Type	K	Spr.1	Spr.2	Spr.3	Spr.4	Spr.5	Spr.6	Spr.7	Spr.8	Spr.9	Spr.10	ITM	OTM	Total
Put	−2.00	–	–	–	–	–	–	–	0.141	–	–	–	1	1
	−1.50	–	–	–	–	–	–	–	0.202	–	–	–	1	1
	−1.25	–	–	–	–	–	–	–	0.256	–	–	–	1	1
	−1.00	–	–	–	–	–	–	–	0.337	–	–	1	–	1
Call	−1.00	–	–	–	–	–	–	–	0.278	–	–	–	1	1
	−0.75	–	–	–	–	–	–	–	0.143	–	–	–	1	1
	−0.50	–	–	–	–	–	–	–	0.055	–	–	–	1	1
	−0.25	–	–	–	–	–	–	–	0.013	–	–	–	1	1
ITM		–	–	–	–	–	–	–	1	–	–	1		
OTM		–	–	–	–	–	–	–	7	–	–		7	
Total		–	–	–	–	–	–	–	8	–	–			8

(c) ULSD

Type	K	Spr.1	Spr.2	Spr.3	Spr.4	Spr.5	Spr.6	Spr.7	Spr.8	Spr.9	Spr.10	ITM	OTM	Total
Spread	–	0.0357	0.0579	–	–	–	–	–	–	–	–	–	–	–
Put	0.00	0.0166	–	–	–	–	–	–	–	–	–	–	1	1
	0.07	0.0543	0.0674	–	–	–	–	–	–	–	–	2	–	2
	0.20	0.1673	0.1571	–	–	–	–	–	–	–	–	2	–	2
	0.25	0.2161	–	–	–	–	–	–	–	–	–	1	–	1
	0.35	0.3151	–	–	–	–	–	–	–	–	–	1	–	1
	0.55	0.5141	–	–	–	–	–	–	–	–	–	1	–	1
Call	0.00	0.0523	–	–	–	–	–	–	–	–	–	1	–	1
	0.07	0.0201	0.0560	–	–	–	–	–	–	–	–	–	2	2
	0.20	0.0034	0.0165	–	–	–	–	–	–	–	–	–	2	2
	0.25	0.0023	–	–	–	–	–	–	–	–	–	–	1	1
	0.35	0.0016	–	–	–	–	–	–	–	–	–	–	1	1
	0.55	0.0010	–	–	–	–	–	–	–	–	–	–	1	1
ITM		6	2	–	–	–	–	–	–	–	–	8		
OTM		6	2	–	–	–	–	–	–	–	–		8	
Total		12	4	–	–	–	–	–	–	–	–			16

Notes: In this table, we present all quoted CSO prices associated with selected spreads from Table 4 (highlighted in gray): for WTI, we report prices for ten 1M spreads; for HH, CSO prices are available for the eighth 3M spread; and for ULSD, we report prices for the first and second 1M spreads. ATM and OTM option prices are shown in gray. WTI prices are quoted in USD/barrel, HH prices in USD/MMBtu, and ULSD prices in USD/gallon.

4.2. Descriptive insights and price dynamics

For each benchmark, we analyze one year of historical data, spanning from June 1, 2022 to May 31, 2023. Fig. 1 presents futures prices for different maturities: F1, F2, F4, F7, and F13. Fig. 2 displays spread prices for 1M, 3M, 6M, and 12M contracts. The futures time series for the three benchmarks frequently exhibit jumps, primarily due to temporary imbalances between supply and demand (see, e.g., D'Ecclesia et al., 2014 for crude oil) or economic news affecting the market. The presence of jumps in futures prices and spreads can be observed in both figures. Also well-known stylized fact in energy markets is that near-maturity futures tend to be more volatile than long-term ones, resulting in larger spreads for longer maturities. This pattern is clearly observable in the figures, where spreads vary in both sign and magnitude. Fig. 3 depicts front-month (F1) futures prices alongside the corresponding ATM implied volatilities, with obvious signs of stochastic behavior. The leverage effect, that is, a negative correlation between price and volatility, is apparent in crude oil and heating oil. In contrast, natural gas exhibits the so-called inverse leverage effect. Over the observation period, the correlations between log-price and volatility changes are for WTI, −62.11%; HH, 15.32%; and ULSD, −12.94%. Overall, this evidence supports the use of jump and stochastic volatility models.

We further examine the term structure of futures prices and spreads as observed on February 8, 2023. Fig. 4 illustrates this structure across 36 rolled-over monthly contracts. As shown in Fig. 4(a), the crude oil market is predominantly in backwardation, a downward-sloping term structure, except for the first two contracts (F1 and F2) which are in contango (upward-sloping). In backwardation, current inventories are valued more highly than deferred deliveries, discouraging storage. Conversely, in contango, holding inventory for future sale can yield a premium, net of storage costs. Fig. 4(b) reveals that natural gas is in contango, with a strong seasonal component. The winter season (November–March), known as the withdrawal phase, is characterized by heightened volatility, while the summer season (April–October), the injection phase, is typically more stable.

Due to elevated demand during winter, those contracts often trade at a premium, resulting in local backwardation, while summer contracts tend to exhibit contango. The 3M CSO analyzed in our study (see Table 6b) corresponds to the October–January spread (Spr.8), which coincides with the first trough in the red dotted line of Fig. 4(b). Finally, Fig. 4(c) shows that ULSD futures exhibit consistent backwardation across all maturities.

4.3. Model calibration

We implement calibration between market and model prices in two steps.

In the first step, we calibrate all model parameters except for the correlation between the two futures. The objective function is constructed using prices of European PVOs written on each of the two futures forming the spread. Specifically, we solve

$$\min_{\bar{\sigma}_1,\bar{\sigma}_2,\phi}\left\{\sum_{i=1}^{N_1}\left[\frac{p_{\text{PVO}}(K_i,T_1)-\hat{p}_{\text{PVO}}(K_i,T_1;\bar{\sigma}_1,\phi)}{\mathcal{V}^2(K_i,T_1)}\right]^2+\sum_{i=1}^{N_2}\left[\frac{p_{\text{PVO}}(K_i,T_2)-\hat{p}_{\text{PVO}}(K_i,T_2;\bar{\sigma}_2,\phi)}{\mathcal{V}^2(K_i,T_2)}\right]^2\right\}, \tag{4.1}$$

where p_{PVO} and $\hat{p}_{\text{PVO}}$ denote the market and model option prices weighted by squared Black vegas $\mathcal{V}$ (see Cont and Tankov, 2004) evaluated at the implied volatilities of the market option prices, N_1 and N_2 are the number of PVOs/strikes for the first and second futures, and $\bar{\sigma}_1$ and $\bar{\sigma}_2$ for the first and second futures are for Group 1 models $\bar{\sigma}_j=\sigma_{F_j}$; for the ST18 model $\bar{\sigma}_j=\{\alpha_j,\gamma_j\}$. ϕ is the vector of remaining model parameters: for the stochastic volatility process, $\phi=\{\theta,\kappa,\sigma_V,V_0,\rho_{FV}\}$; for the compound Poisson process, $\phi=\{\mu_J,\sigma_J,\lambda\}$. PVO model prices for all Group 1 models and the ST18 model are computed with high accuracy using, respectively, the COS method (Fang and Oosterlee, 2008) and conditional Monte Carlo simulation. For the latter, we rely on the fact that the futures log-price follows a normal distribution conditional on a path of the variance process, which allows the Black formula to be nested within the pricing expectation (see also related discussion in Section 3.3).

In the second step, we calibrate only the correlation parameter ρ between the two futures, keeping all other parameters fixed at the values obtained in the first step. The objective function is based on CSO prices and reads

$$\min_{\rho}\sum_{i=1}^{N}\left[p_{\text{CSO}}(K_i,T_1,T_2)-\hat{p}_{\text{CSO}}(K_i,T_1,T_2;\bar{\sigma}_1,\bar{\sigma}_2,\phi,\rho)\right]^2, \tag{4.2}$$

where N is the number of CSOs/strikes for a given spread. As a proxy for the CSO model prices $\hat{p}$, we use the very accurate lower bound LB_{CSO} in Eq. (3.4) for Group 1 models, computed using Gauss–Kronrod quadrature with suitably chosen damping parameter δ. The relevant joint characteristic function is provided in Eq. (3.6). Although the exact same approach can be applied to ST18, we instead adhere to the conditional Monte Carlo approach outlined in Section 3.3, for the reasons explained therein.

Ultimately, to assess model fit, we compute three standard error metrics: the mean error (ME), the mean absolute error (MAE), and the root mean squared error (RMSE), defined as

$$\text{ME}=\frac{1}{N}\sum_{i=1}^{N}\left(\hat{p}^i-p^i\right),\ \text{MAE}=\frac{1}{N}\sum_{i=1}^{N}\left|\hat{p}^i-p^i\right|,\ \text{RMSE}=\sqrt{\frac{1}{N}\sum_{i=1}^{N}\left(\hat{p}^i-p^i\right)^2}. \tag{4.3}$$

5. Model results and analysis

In what follows, we present the results of our empirical analysis, based on the calibration of our pool of models to the market data described in Section 4. All models listed in Section 3 are calibrated following the procedure outlined in Section 4.3. In summary, we recall that the models are calibrated on PVOs written individually on the two futures composing the spread. The correlation coefficient between the two futures (in log scale) is then estimated based on the CSO quotes. In particular, we use different term contracts depending on the benchmark: for WTI, the 1M CSO contracts are the most liquid; for HH (ULSD), the most liquid CSO contract is the 3M (1M). The resulting parameter estimates are reported in Table 7, with the associated PVO fitting error statistics provided in Table 8.

From our PVO calibration results, it is evident that stochastic volatility models consistently outperform. For WTI, the Bat96 model improves upon Hes93 for the first two maturities: introducing jumps enhances the fit for short maturities, while stochastic volatility has a more pronounced impact on longer maturities. Since the Mer76 model performs worse than Hes93 across all maturities, the combination with stochastic volatility appears essential. For HH, where we have options of only one short maturity, the Mer76 and Bat96 models outperform Hes93; however, this may be less representative due to the limited number of contracts. For ULSD, all models yield very low RMSEs, making it difficult to distinguish a clearly superior model. In terms of the correlation between log-returns and volatility increments, we observe sign differences for HH (negative in Hes93, positive in Bat96), whereas for WTI both models produce negative correlation and for ULSD both produce positive correlation.

For HH, the ST18 model significantly improves upon Hes93 by halving the RMSE; moreover, volatility for the shorter-dated future is larger than that for the longer-dated one ($\gamma_2>\gamma_1$). In contrast, WTI, which is not a seasonal commodity, does not exhibit a consistent Samuelson pattern, with γ_j, $j=1,2$, being practically zero overall. Hence, ST18 tends to revert to the Hes93 model in this case. For ULSD, although a Samuelson effect is clearly present, the impact on the RMSE is marginal as said earlier.

Having obtained the parameters by calibrating to PVO market prices, we next compare the resulting model CSO prices with corresponding market prices. From Table 7, we first observe that the implied correlation from WTI CSO prices is equal to 1 across all contracts and models. Note that this refers to the correlation between log-futures prices; even when this correlation is perfect, the spread of futures prices retains some volatility, and the corresponding option has nonzero time value. For HH and ULSD, the implied correlation differs slightly across models and is above 0.90. These high correlations can be attributed to the narrow maturity gaps of the futures forming each spread. Some further insight is provided in Fig. 5 (illustratively for Hes93 only, and computed using 2D FFT), which displays the marginal and joint probability densities of the futures underlying the spreads for each benchmark. While the bivariate densities are quite concentrated, reflecting the high correlations, this does not imply vanishing volatility in the spread itself.

A few comments are in order based on Table 9, which presents the CSO pricing errors across different CSO maturities and commodities. For WTI, Mer76 exhibits the weakest performance overall, particularly for longer-dated CSOs (e.g., RMSE reaches 5.1665 for CSO 10). A consistently high negative ME across CSOs 4–10 indicates a strong downward pricing bias. Bat96 shows mixed performance, with errors increasing with maturity. RMSE ranges from 0.0130 to 0.1204 (mid- to long-term CSOs), and ME similarly shows a mild negative bias. While the model performs reasonably

Table 7
Calibrated models.

(a) WTI

Model	Param.	Spr.1	Spr.2	Spr.3	Spr.4	Spr.5	Spr.6	Spr.7	Spr.8	Spr.9	Spr.10
Bla76	σ_1	0.2325	0.3349	0.366	0.3798	0.3848	0.3883	0.3878	0.387	0.383	0.3811
	σ_2	0.3349	0.366	0.3798	0.3848	0.3883	0.3878	0.387	0.383	0.3811	0.3791
	ρ	1	1	1	1	1	1	1	1	1	1
Mer76	σ_1	0.2158	0.3038	0.3282	0.3368	0.3366	0.3322	0.317	0.3281	0.2633	0.3083
	σ_2	0.3054	0.3293	0.338	0.3388	0.3372	0.3294	0.3142	0.3244	0.2578	0.3028
	ρ	1	1	1	1	1	1	1	1	1	1
	λ	0.1746	0.1415	0.1339	0.1126	0.1009	0.1646	0.2793	0.1143	0.6364	0.1869
	μ_J	−0.4827	−0.6633	−0.734	−0.9341	−1.1321	−0.7159	−0.5216	−1.0515	−0.3987	−0.7148
	σ_J	0.26	0.3161	0.349	0.4021	0.4129	0.3672	0.151	0.5229	0.0392	0.3478
Hes93	σ_1	0.4604	0.4451	0.4645	0.4802	0.474	0.4842	0.4793	0.4875	0.4857	0.4922
	σ_2	0.4161	0.4488	0.4584	0.4843	0.4808	0.4828	0.474	0.488	0.4827	0.4906
	ρ	1	1	1	1	1	1	1	1	1	1
	V_0	0.002	0.353	0.4061	0.5824	0.6705	0.6051	0.5292	0.6537	0.6349	0.6505
	σ_V	3.6371	1.1831	0.8796	0.8624	0.7914	0.8333	0.8307	0.4733	0.5247	0.6441
	κ	5	4.3438	2.6708	1.3681	0.658	1.2307	1.7234	0.1506	0.5922	1.9709
	θ	2.5556	1.2707	1.3273	0.8801	0.7156	0.8638	0.9631	0.6413	0.7717	0.568
	ρ_{FV}	−0.28	−0.7537	−0.8696	−0.677	−0.6719	−0.7119	−0.808	−0.9634	−0.9915	−0.6605
Bat96	σ_1	0.3409	0.4596	0.4973	0.514	0.5213	0.5215	0.5148	0.5081	0.5208	0.5165
	σ_2	0.4936	0.5073	0.5202	0.5243	0.5298	0.5246	0.5156	0.5177	0.5187	0.5144
	ρ	1	1	1	1	1	1	1	1	1	1
	V_0	0.4047	0.4965	0.5022	0.5293	0.5395	0.54	0.5379	0.7951	0.5357	0.5504
	σ_V	0.6776	0.5169	0.5368	0.6863	0.6687	0.6496	0.6147	0.4707	0.4639	0.5733
	κ	2.3897	1.5078	2.0582	0.8198	0.319	1.0548	1.4464	0.9425	0.074	1.179
	θ	0.4004	0.3723	0.4556	0.4594	0.4763	0.4719	0.4767	0	0.4557	0.1432
	ρ_{FV}	−0.9099	−0.9133	−0.9227	−0.6638	−0.6714	−0.7521	−0.8171	−1	−0.8953	−0.716
	λ	0.7517	0.2589	0.2455	0.248	0.2688	0.3126	0.3343	0.1913	0.3011	0.3106
	μ_J	−0.0176	−0.2044	−0.2329	−0.1636	−0.1242	−0.1814	−0.219	−0.0249	−0.1745	−0.1565
	σ_J	0.1525	0.0917	0.0521	0.1107	0.0921	0.1027	0.1172	0.0061	0.0962	0.0942
ST18	α_1	0.461	0.4448	0.4646	0.4802	0.474	0.4844	0.488	0.4879	0.4857	0.4844
	α_2	0.4158	0.4487	0.4586	0.4841	0.4807	0.4829	0.4758	0.5337	0.4826	0.4826
	γ_1	0.0001	0	0	0	0.0001	0.0001	0.00387	0	0	0
	γ_2	0	0	0.0001	0	0.0001	0.0001	0.0001	0.00585	0	0.0001
	ρ	1	0.965	0.96	0.965	0.965	0.965	1	1	0.9	0.965
	V_0	0.002	0.353	0.4061	0.5824	0.6705	0.6051	0.5292	0.6537	0.6349	0.6505
	σ_V	3.6371	1.1831	0.8796	0.8624	0.7914	0.8333	0.8307	0.4733	0.5247	0.6441
	κ	5	4.3438	2.6708	1.3681	0.658	1.2307	1.7234	0.1506	0.5922	1.9709
	θ	2.5556	1.2707	1.3273	0.8801	0.7156	0.8638	0.9631	0.6413	0.7717	0.568
	ρ_{FV}	−0.28	−0.7537	−0.8696	−0.677	−0.6719	−0.7119	−0.808	−0.9634	−0.9915	−0.6605

(b) HH

Model	Param.	Spr.8
Bla76	σ_1	0.6027
	σ_2	0.5746
	ρ	0.915
Mer76	σ_1	0.3035
	σ_2	0.0833
	ρ	1
	λ	1.6749
	μ_J	−0.3715
	σ_J	0.3364
Hes93	σ_1	0.4728
	σ_2	0.4218
	ρ	0.9
	V_0	0.001
	σ_V	2.2822
	κ	4.9983
	θ	2.5935
	ρ_{FV}	−0.9501
Bat96	σ_1	0.3485
	σ_2	0.082
	ρ	1
	V_0	0.4282
	σ_V	1.2586
	κ	3.1104
	θ	0.9146
	ρ_{FV}	0.7708
	λ	1.5435
	μ_J	−0.3883
	σ_J	0.3623
ST18	α_1	0.4696
	α_2	0.402
	γ_1	0.0001
	γ_2	0.0622
	ρ	1
	V_0	0.001
	σ_V	2.2822
	κ	4.9983
	θ	2.5935
	ρ_{FV}	−0.9501

(c) ULSD

Model	Param.	Spr.1	Spr.2
Bla76	σ_1	0.3379	0.3642
	σ_2	0.3642	0.3725
	ρ	0.935	0.92
Mer76	σ_1	0.3293	0.3256
	σ_2	0.3421	0.3196
	ρ	0.965	0.995
	λ	0.0708	0.1426
	μ_J	0.5471	0.5193
	σ_J	0.2156	0.3938
Hes93	σ_1	0.4638	0.4559
	σ_2	0.4797	0.4554
	ρ	0.925	0.905
	V_0	0.4977	0.6021
	σ_V	2.4725	4.2577
	κ	1.9992	1.7912
	θ	1.3478	1.7451
	ρ_{FV}	0.2707	0.3619
Bat96	σ_1	0.4662	0.4704
	σ_2	0.4864	0.4794
	ρ	0.935	0.96
	V_0	0.4986	0.5175
	σ_V	1.198	1.617
	κ	1.741	1.3089
	θ	1.097	0.9549
	ρ_{FV}	0.1791	0.611
	λ	0	0.1559
	μ_J	−0.003	−0.3856
	σ_J	0.01	0.025
ST18	α_1	0.5036	0.4803
	α_2	0.4844	0.476
	γ_1	0.7743	1.0256
	γ_2	1.048	1.0365
	ρ	0.935	0.915
	V_0	0.4977	0.6021
	σ_V	2.4725	4.2577
	κ	1.9992	1.7912
	θ	1.3478	1.7451
	ρ_{FV}	0.2707	0.3619

Notes: This table presents the calibrated parameter values for all models, reported separately for each underlying.

Table 8
PVO pricing errors.

(a) WTI

Model	Spr.1	Spr.2	Spr.3	Spr.4	Spr.5	Spr.6	Spr.7	Spr.8	Spr.9	Spr.10
Bla76	0.0983	0.1384	0.1546	0.1679	0.1835	0.1963	0.2014	0.2039	0.2232	0.2321
Mer76	0.0108	0.0120	0.0107	0.0096	0.0100	0.0082	0.0059	0.0076	0.0089	0.0092
Hes93	0.0077	0.0031	0.0022	0.0027	0.0027	0.0022	0.0024	0.0024	0.0029	0.0056
Bat96	0.0035	0.0028	0.0023	0.0027	0.0027	0.0022	0.0024	0.0023	0.0028	0.0061
ST18	0.0077	0.0031	0.0022	0.0027	0.0027	0.0022	0.0024	0.0022	0.0029	0.0056

(b) HH

Model	Spr.8
Bla76	0.0425
Mer76	0.0020
Hes93	0.0235
Bat96	0.0017
ST18	0.0101

(c) ULSD

Model	Spr.1	Spr.2
Bla76	0.0012	0.0042
Mer76	0.0004	0.0004
Hes93	0.0003	0.0004
Bat96	0.0007	0.0002
ST18	0.0003	0.0003

Notes: This table reports the RMSE, defined in Eq. (4.3), for pricing PVOs across three energy commodities, covering all models.

well in the short- to mid-term, it tends to underperform for longer maturities, due to possible overfitting during the PVO calibration. On the other hand, Hes93 achieves the best overall performance. It delivers the lowest RMSE across all CSOs, with results that are consistent and stable. RMSE ranges from 0.0146 to 0.0496, with an average of 0.0383. ME values are close to zero, indicating no significant bias. Furthermore, ST18 performs equally well, as the two additional parameters have negligible influence in the PVO calibration for the considered markets. Lastly, Bla76, despite being a constant-volatility model, performs competitively, especially in short- and mid-term contracts, with an overall RMSE of 0.0449. ME and MAE are small, indicating no major pricing bias. For HH, Hes93 and ST18 remain the best-performing models, followed by Bla76. For ULSD, Bla76 outperforms Bat96, ST18, and Hes93, which exhibit similar RMSE levels. This observation aligns with market practice, where simpler models are often used even for relatively complex derivatives such as CSOs. Contrary to the PVO market, the CSO market is considerably smaller attracting fewer advanced operators (see the relevant discussion in the introduction of the paper and Table 1, which reports the open interest in energy options on NYMEX).

6. Conclusion

In this paper, we derive expressions for the joint characteristic function of log-futures prices under a broad class of affine models, accommodating both stochastic volatility and jumps, as well as time-dampening features when present. In addition, we introduce a novel methodology based on

(a) WTI

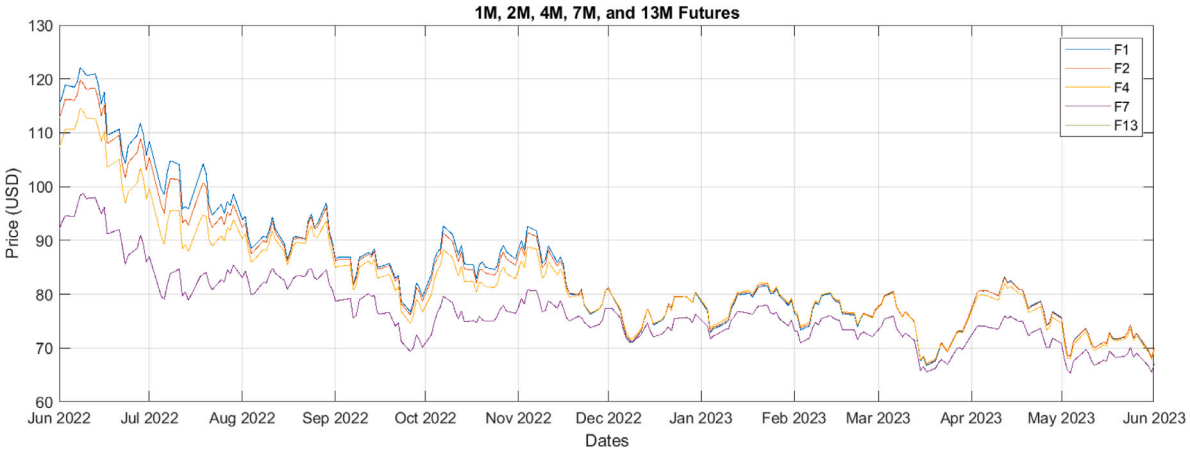

(b) HH

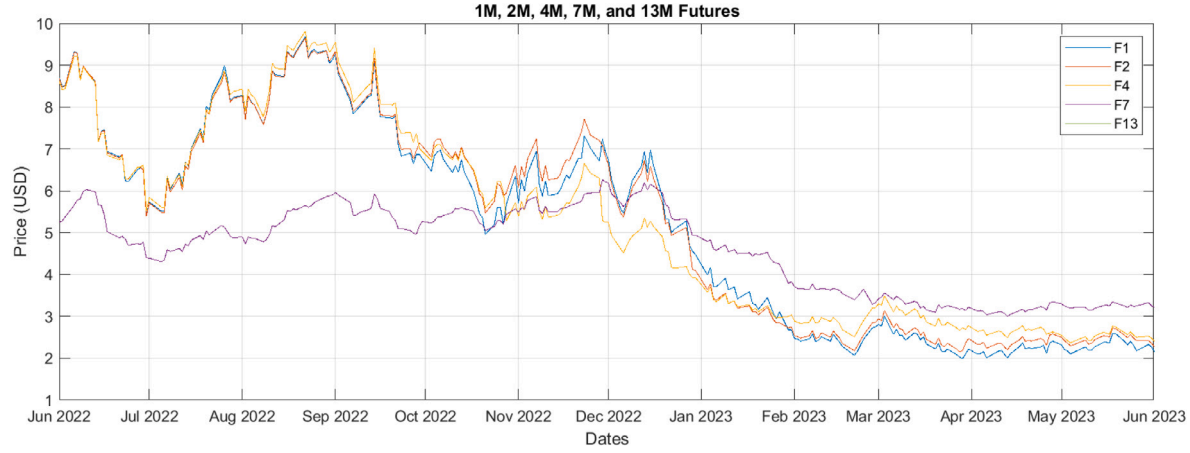

(c) ULSD

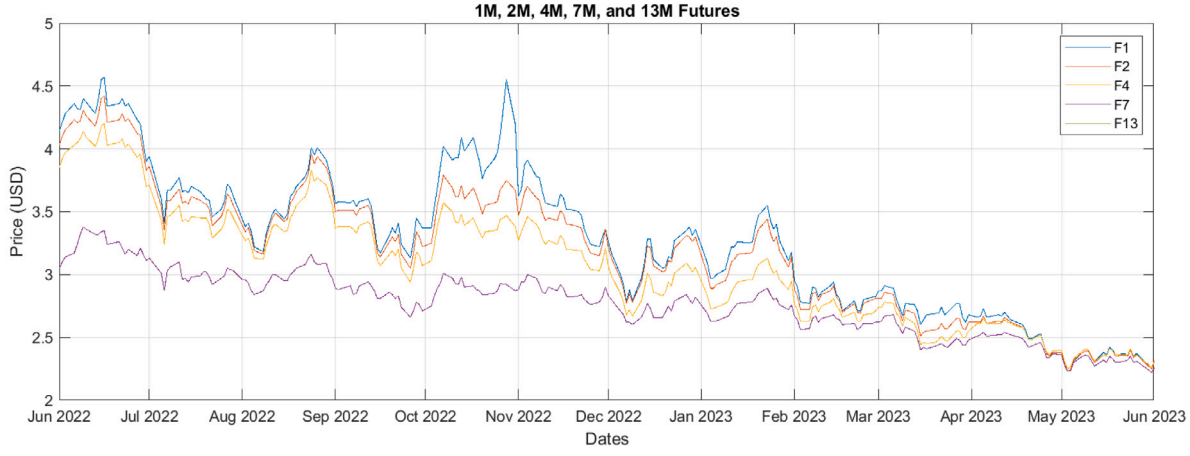

Fig. 1. Time series of futures prices.
Notes: Each figure displays price plots (in USD) for five different futures contracts for WTI, HH, and ULSD.

a conditioning arguments for pricing spread options under advanced stochastic volatility models, such as ST18, where computing the bivariate characteristic functions typically poses significant computational challenges. Our unified approach enables model calibration and provides a tractable, consistent framework for pricing calendar spread options on energy commodities.

Our empirical analysis, based on market data, focuses on three major energy benchmarks: WTI crude oil, Henry Hub natural gas, and ULSD heating oil. We calibrate each model to the prices of PVOs and subsequently to CSO quotes, using a two-step procedure. The results show that stochastic volatility models, particularly Hes93 and ST18, offer superior performance in fitting PVO prices. The inclusion of jumps improves the fit

(a) WTI

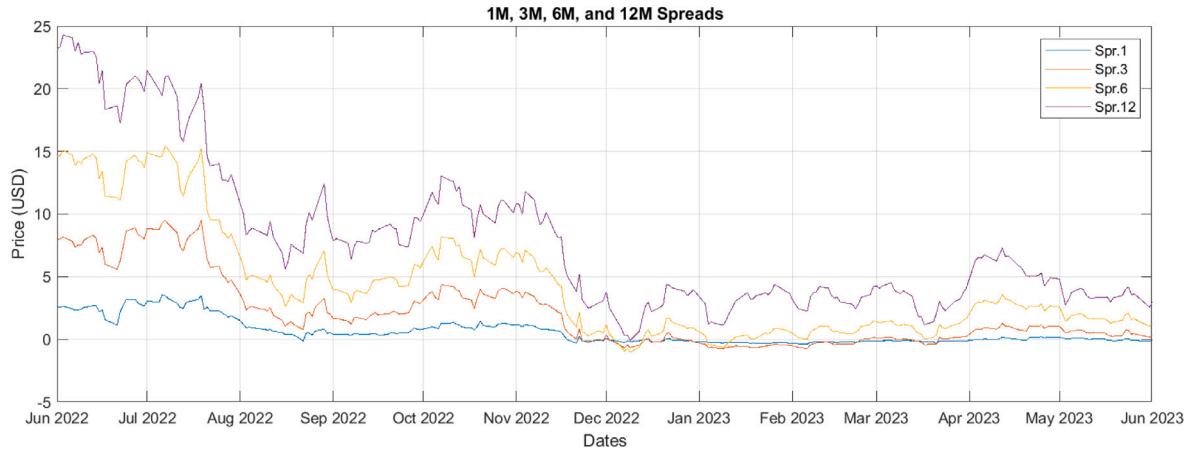

(b) HH

(c) ULSD

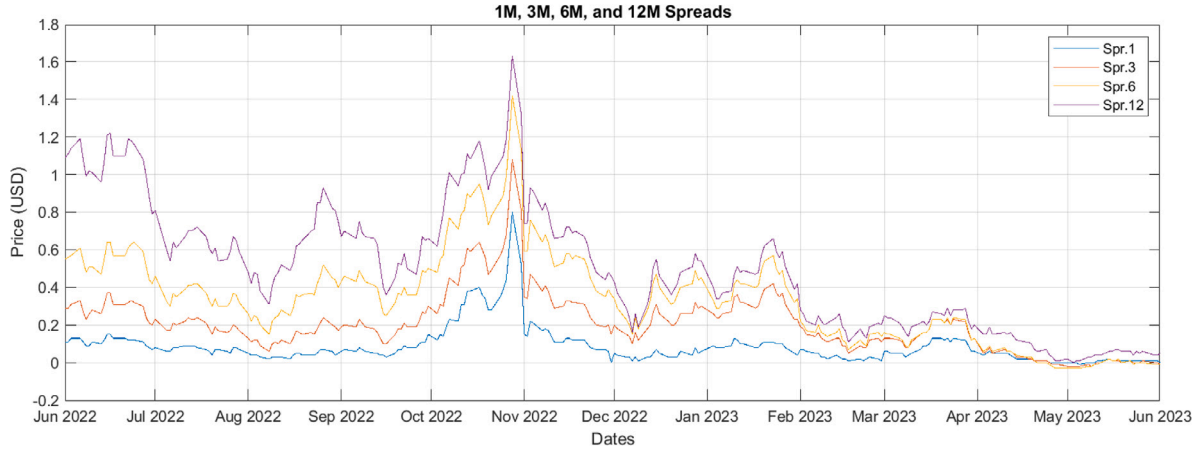

Fig. 2. Time series of spreads.
Notes: Each figure displays spread plots (in USD) for four different contracts for WTI, HH, and ULSD.

for short maturities, while stochastic volatility is especially effective for longer maturities. When evaluating CSO pricing errors, the Hes93 model consistently delivers the lowest RMSE and minimal bias across contracts, with ST18 performing equally well. In contrast, the Mer76 model exhibits the weakest fit, particularly for long-dated spreads. Interestingly, the Bla76 model performs competitively for short- and mid-term contracts, in line with market practices that favor parsimonious models for CSO trading.

Future research could extend this framework to other types of spread options, and explore more explicitly the effects of seasonality and storage costs within the modeling setup.

(a) WTI

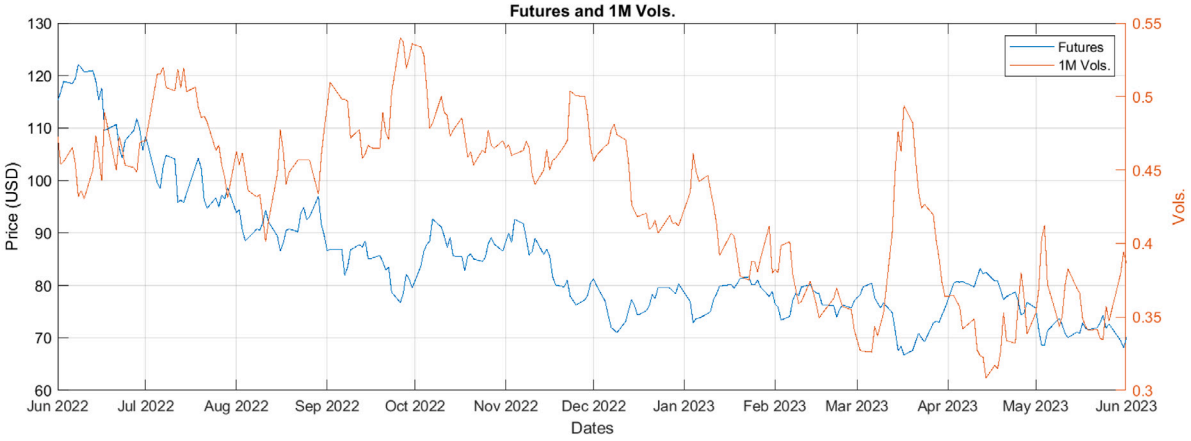

(b) HH

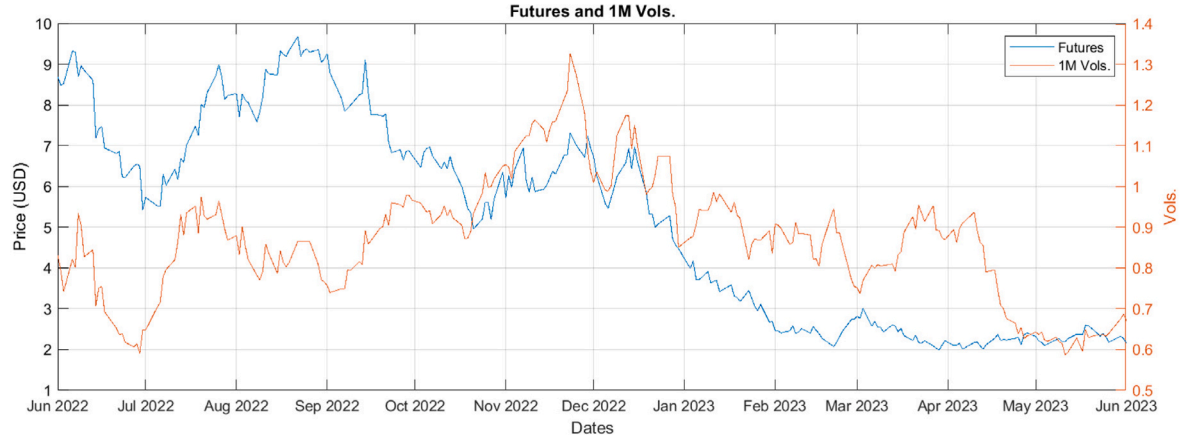

(c) ULSD

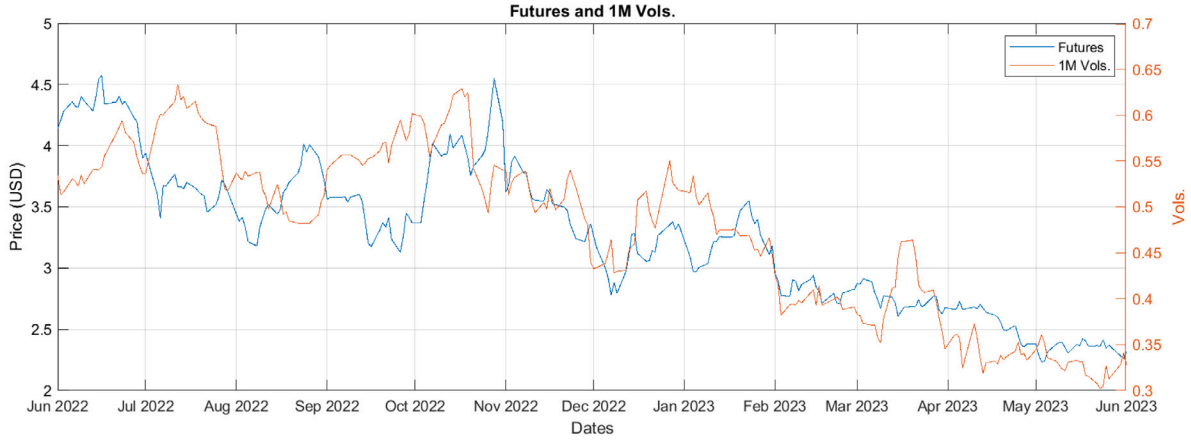

Fig. 3. Time series — front contract futures prices and volatilities.
Notes: The figures display the front futures prices and the 30-day ATM implied volatilities for WTI, HH, and ULSD. Prices (left vertical axis) are expressed in USD, while volatilities (right vertical axis) are expressed in decimal form.

CRediT authorship contribution statement

Carme Frau: Writing – review & editing, Writing – original draft, Visualization, Software, Resources, Project administration, Methodology, Investigation, Formal analysis, Data curation. **Gianluca Fusai:** Writing – review & editing, Validation, Supervision, Methodology, Investigation, Formal analysis, Conceptualization. **Ioannis Kyriakou:** Writing – review & editing, Validation, Supervision, Project administration, Methodology, Investigation, Formal analysis.

(a) WTI

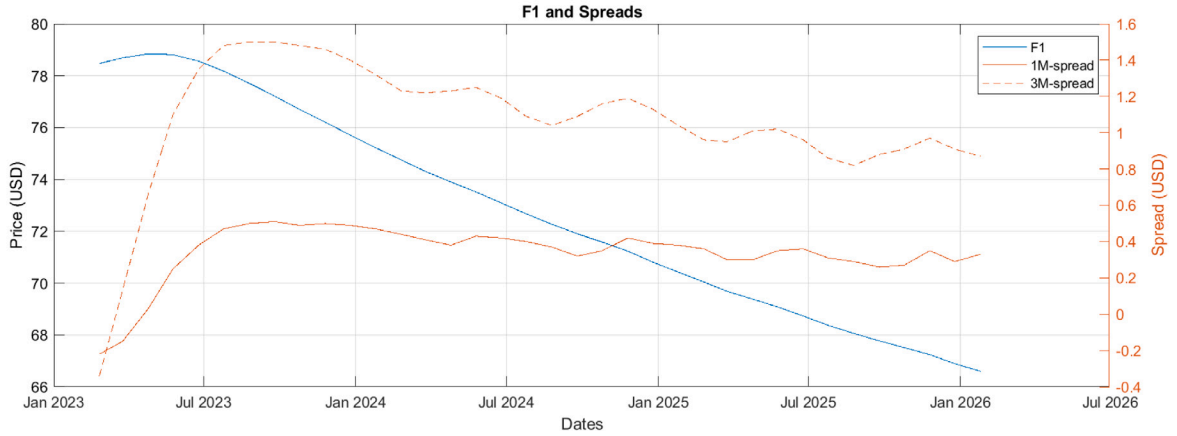

(b) HH

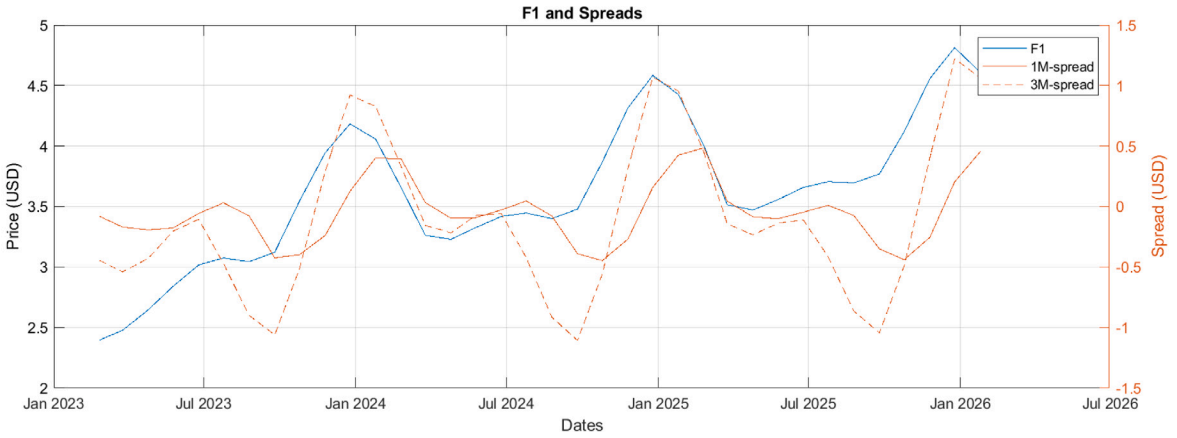

(c) ULSD

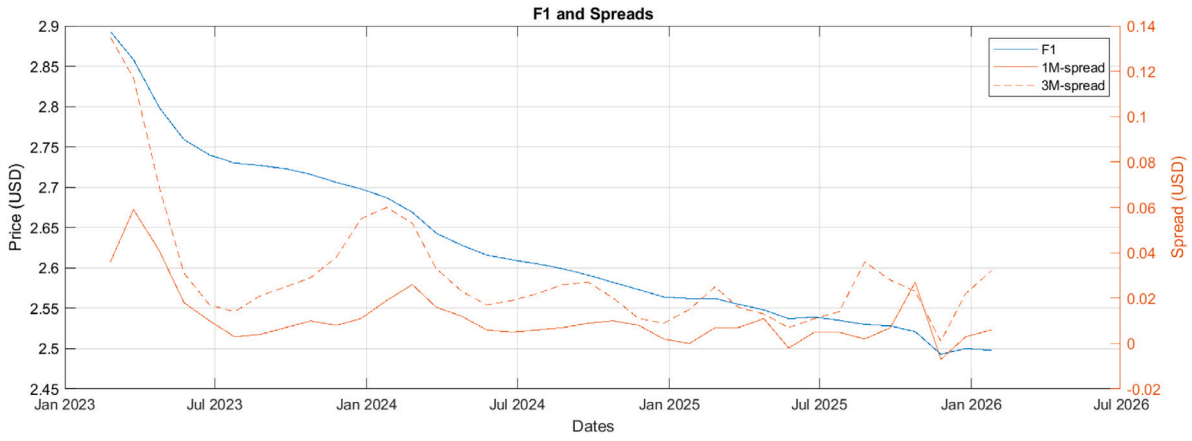

Fig. 4. Term structures — futures prices and spreads.
NOTES: In this figure, we present the term structure of futures contracts, as well as the 1M and 3M spreads for WTI, HH, and ULSD, across 36 consecutive contract months. The observation date is February 8, 2023. Along the horizontal axis, we indicate the contract maturity (first maturity corresponds to February 2023 and first contract month is March 2023).

Acknowledgement

We are grateful to the editors and anonymous reviewers for their fruitful suggestions and helpful comments. Any remaining errors are our own. We have all reviewed the results and approved the final version of the manuscript. During the preparation of this article, Carme Frau was initially affiliated with the Department of Economic Analysis and Quantitative Economics, Universidad Complutense de Madrid (Spain). She wants to thank Lorenz Schneider and Ilia Bouchouev for various fruitful discussions and constructive comments, Lola Robles, John Crosby, and the participants at Finance Forum 2022, Energy Finance Italy EFI8 2023, UIB's DEE research seminar 2023, the 2023 edition of the anual meeting of Commodity

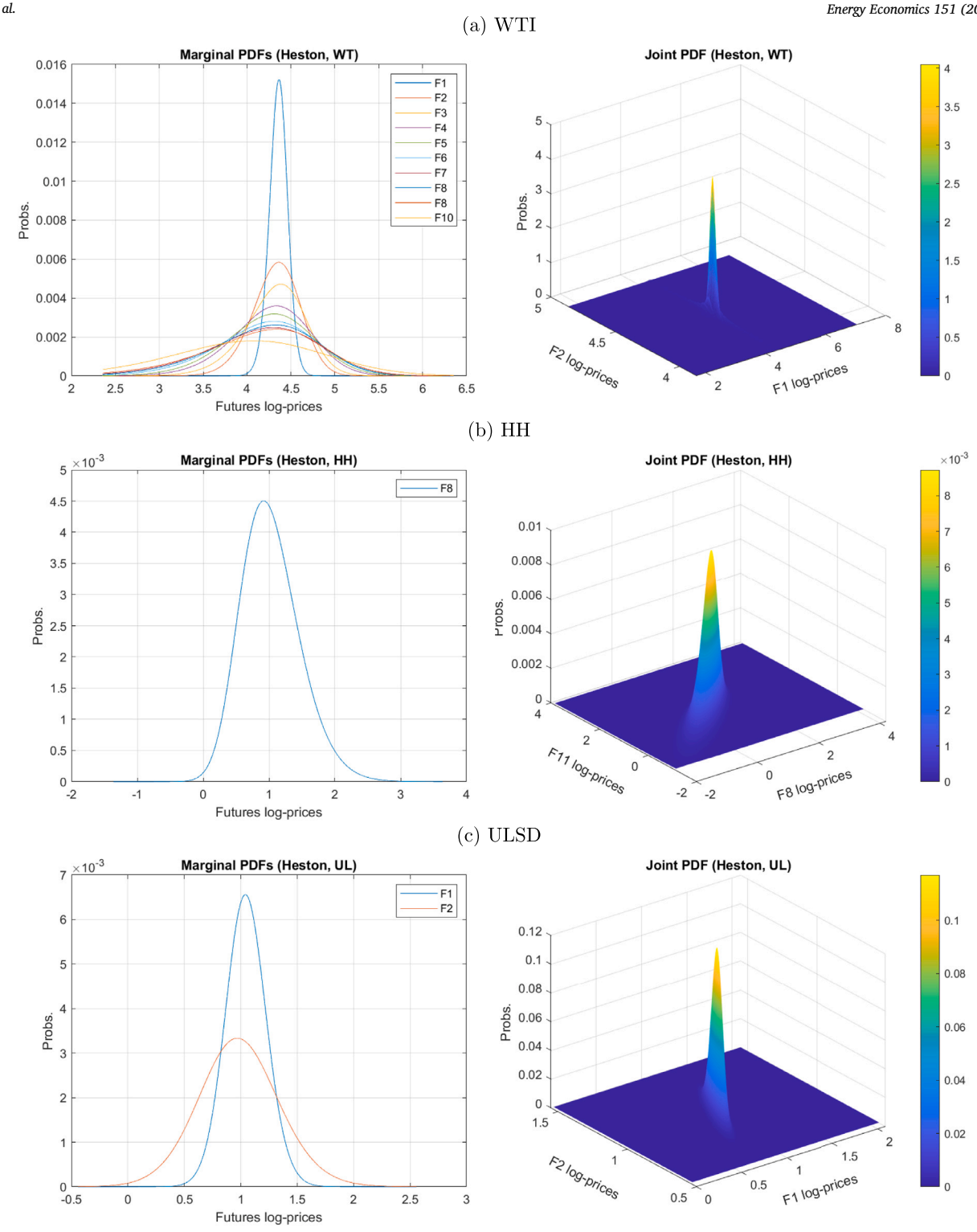

Fig. 5. Futures log-price densities under the Hes93 model.
NOTES: In these figures, we present the marginal and joint PDFs of the futures log-prices for the three benchmarks under the Hes93 model.

and Energy Markets Association (CEMA), the II Jornada de Mercados Financieros del Banco de España 2023, Energy Finance Italy EFI9 2024, 31st Global Finance Conference 2024, and the QUANT research seminar at Emlyon Business School (2024), for their helpful comments and suggestions.

Appendix A. Joint characteristic function of log-futures prices

Consider the bivariate transform involving the spread $s(t, T_1, T_2)$ in Eq. (3.3)

$$\boldsymbol{\Phi}_{\mathbf{F}}(u_1, u_2) = \mathbb{E}_t^{\mathbb{Q}}\left[e^{iu_1 \ln F(T_0,T_1)+iu_2 \ln F(T_0,T_2)}\right]. \tag{A.1}$$

Table 9
CSO pricing errors.

(a) WTI

Model	Stat.	Spr.1	Spr.2	Spr.3	Spr.4	Spr.5	Spr.6	Spr.7	Spr.8	Spr.9	Spr.10
Bla76	ME	−0.0460	−0.0172	0.0029	0.1283	0.0067	0.0050	0.0030	0.0050	0.0052	0.0037
	MAE	0.0519	0.0367	0.0210	0.1283	0.0553	0.0285	0.0471	0.0349	0.0508	0.0401
	RMSE	0.0757	0.0424	0.0230	0.1379	0.0595	0.0328	0.0516	0.0395	0.0577	0.0449
Mer76	ME	−0.1300	−0.4882	0.0029	−1.1629	−1.3726	−1.6879	−3.4684	−2.4918	−3.8305	−5.1662
	MAE	0.1300	0.4882	0.0210	1.1629	1.3726	1.6879	3.4684	2.4918	3.8305	5.1662
	RMSE	0.1325	0.4888	0.0230	1.1636	1.3749	1.6885	3.4690	2.4925	3.8310	5.1665
Hes93	ME	−0.0011	0.0067	0.0024	0.0034	0.0059	0.0044	0.0028	0.0048	0.0051	0.0036
	MAE	0.0121	0.0265	0.0126	0.0185	0.0417	0.0191	0.0405	0.0326	0.0435	0.0341
	RMSE	0.0177	0.0283	0.0146	0.0217	0.0451	0.0236	0.0443	0.0368	0.0496	0.0383
Bat96	ME	−0.0134	0.0067	0.0023	−0.0967	−0.0919	−0.0892	−0.0353	−0.2883	−0.0246	−0.1081
	MAE	0.0139	0.0263	0.0112	0.0967	0.0919	0.0892	0.0497	0.2883	0.0415	0.1081
	RMSE	0.0248	0.0282	0.0130	0.1008	0.1166	0.0995	0.0681	0.2931	0.0604	0.1204
ST18	ME	−0.0005	−0.0326	0.0193	−0.0656	−0.1087	−0.1156	−0.1528	−0.1968	−0.0064	−0.0871
	MAE	0.0115	0.0326	0.0242	0.0656	0.1087	0.1156	0.1653	0.1968	0.0613	0.0881
	RMSE	0.0002	0.0015	0.0008	0.0045	0.0159	0.0148	0.0353	0.0511	0.0050	0.0106

(b) HH

Model	Stat.	Spr.8
Bla76	ME	−0.0013
	MAE	0.0013
	RMSE	0.0264
Mer76	ME	−0.0479
	MAE	0.0479
	RMSE	0.0486
Hes93	ME	0.0142
	MAE	0.0142
	RMSE	0.0166
Bat96	ME	−0.0382
	MAE	0.0382
	RMSE	0.0389
ST18	ME	−0.0121
	MAE	0.0121
	RMSE	0.0152

(c) ULSD

Model	Stat.	Spr.1	Spr.2
Bla76	ME	0.0011	0.0003
	MAE	0.0017	0.0005
	RMSE	0.0019	0.0006
Mer76	ME	−0.0038	−0.0138
	MAE	0.0043	0.0142
	RMSE	0.0046	0.0198
Hes93	ME	0.0010	−0.0010
	MAE	0.0015	0.0021
	RMSE	0.0017	0.0025
Bat96	ME	0.0014	−0.0016
	MAE	0.0017	0.0037
	RMSE	0.0018	0.0041
ST18	ME	0.0013	−0.0009
	MAE	0.0018	0.0021
	RMSE	0.0020	0.0022

NOTES: In this table, we report three error statistics, ME, MAE, and RMSE, defined in Eq. (4.3), for each spread, covering all models.

With $\tau = T_0 - t$, for an affine process with stochastic variance V_t, the JCF is given by Eq. (3.6)

$$\mathbb{E}_t^{\mathbb{Q}}\left[e^{iu_1 f(T_0,T_1)+iu_2 f(T_0,T_2)}\right] = \exp\Big\{ B_1(\tau;u_1,u_2)f(t,T_1) + B_2(\tau;u_1,u_2)f(t,T_2)A(\tau;u_1,u_2) + C(\tau;u_1,u_2)V_t \Big\}. \tag{A.2}$$

With $B_1(\tau,u_1,u_2) = iu_1$, $B_2(\tau,u_1,u_2) = iu_2$, the functions $A(\tau;u_1,u_2)$ and $C(\tau;u_1,u_2)$ satisfy the ODE system

$$\begin{aligned} \frac{\partial A(\tau;u_1,u_2)}{\partial \tau} &= b_0 + \kappa\theta C(\tau;u_1,u_2) + \Lambda(u_1,u_2), \\ \frac{\partial C(\tau;u_1,u_2)}{\partial \tau} &= b_1 C(\tau;u_1,u_2) + b_2 C^2(\tau;u_1,u_2), \end{aligned} \tag{A.3}$$

subject to the initial conditions $A(0;u_1,u_2) = C(0;u_1,u_2) = 0$. The jump components read

$$\begin{aligned} \Lambda(u_1,u_2) &= \sum_{j=1}^{2} \lambda(n_{J_j} - iu_j m_J), \\ m_J = \exp\Big\{\mu_J + \tfrac{1}{2}\sigma_J^2\Big\} - 1, &\qquad n_{J_j} = \exp\Big\{iu_j\mu_J - \tfrac{1}{2}\sigma_J^2 u_j^2\Big\} - 1. \end{aligned} \tag{A.4}$$

For each model in its bivariate form, the ODE terms $\partial A(\cdot)/\partial\tau$, $\partial C(\cdot)/\partial\tau$ can be found in Table 3a, the solutions $A(\cdot), C(\cdot)$ in Table 3b, and the ODE parameters b_0, b_1, b_2 in Table 3c.

A.1. Group 1 models

For $j = 1, 2$, we obtain the following expressions for b_0, b_1, b_2. For the Bla76 and Mer76 models, we have that $C(\cdot) = 0$ and

$$b_0 = -\tfrac{1}{2}\Big(\sum_{j=1}^{2}(u_j^2 + iu_j)\cdot\sigma_{F_j}^2 + 2\rho\prod_{j=1}^{2}u_j\cdot\sigma_{F_j}\Big). \tag{A.5}$$

For the Hes93 and Bat96 models, we additionally have

$$b_1 = -\kappa + \sigma_V\rho_{FV}\sum_{j=1}^{2} iu_j\cdot\sigma_{F_j}, \qquad b_2 = \tfrac{1}{2}\sigma_V^2. \tag{A.6}$$

A.2. Group 2 models

For $j = 1, 2$, we get the following set of results[7]:

$$b_0 = -\frac{1}{2}\left(\sum_{j=1}^{2}(u_j^2 + iu_j)\cdot\sigma_{F_j}^2(t,T_j) + 2\rho\prod_{j=1}^{2}u_j\cdot\sigma_{F_j}(t,T_j)\right), \qquad b_1 = -\kappa + \sigma_V\rho_{FV}\sum_{j=1}^{2}iu_j\cdot\sigma_{F_j}(t,T_j), \qquad b_2 = \tfrac{1}{2}\sigma_V^2. \tag{A.7}$$

The functions $g(z_j)$ and $g'(z_j)$ are linear combinations of Kummer's M and Tricomi's U hypergeometric functions:

$$\begin{aligned} g(z_j) &= k_{1,j}M(a_j,b_j,z_j) + k_{2,j}U(a_j,b_j,z_j),\\ g'(z_j) &= \frac{a_j}{b_j}k_{1,j}M(a_j+1,b_j+1,z_j) - a_jk_{2,j}U(a_j+1,b_j+1,z_j), \end{aligned} \tag{A.8}$$

with coefficients

$$k_{1,j} = \frac{a_j\dfrac{U(a_j+1,b_j+1,\frac{1}{\omega_j})}{U(a_j,b_j,\frac{1}{\omega_j})} - \beta_j\omega_j - \mu_j}{\dfrac{a_j}{b_j}M(a_j+1,b_j+1,\frac{1}{\omega_j}) + a_jM(a_j,b_j,\frac{1}{\omega_j})\dfrac{U(a_j+1,b_j+1,\frac{1}{\omega_j})}{U(a_j,b_j,\frac{1}{\omega_j})}}, \qquad k_{2,j} = \frac{1-k_{1,j}M(a_j,b_j,\frac{1}{\omega_j})}{U(a_j,b_j,\frac{1}{\omega_j})}, \qquad k_{3,j} = -\frac{\mu_j}{\omega_j}. \tag{A.9}$$

Specifically for the ST18 model, we have that[8]

$$a_j = -\left(\mu_jb_j + c_{1,j}\frac{\kappa_j\omega_j}{2\gamma_j}\right), \qquad b_j = 1-\beta_j, \qquad z_j = \frac{e^{-\gamma_j(T_0-t)}}{\omega_j}, \qquad \beta_j = -\frac{c_{0,j}}{\gamma_j}, \qquad \mu_j = -\tfrac{1}{2}\left(1 + c_{1,j}\frac{\omega_j}{\gamma_j}\right), \qquad \omega_j = \frac{\omega^{\pm}\gamma_j}{\sqrt{c_{1,j}^2 - 4d_{2,j}}}, \tag{A.10}$$

where[9] $\omega^{\pm} = -1$ and

$$c_{0,j} = -\kappa, \qquad c_{1,j} = -\sigma_V\rho_{FV}iu_j\cdot\sigma_{F_j}(T_0,T_j), \qquad d_{2,j} = -\tfrac{1}{2}b_2\left((u_j^2+iu_j)\cdot d_{2,y_j} + \tfrac{1}{2}d_{2,12}\right), \qquad d_{2,y_j} = \sigma_{F_j}^2(T_0,T_j), \qquad d_{2,12} = 2\rho\prod_{j=1}^{2}u_j\cdot d_{2,y_j}, \tag{A.11}$$

with $\sigma_{F_j}(T_0,T_j) = \alpha_je^{-\gamma_j(T_j-T_0)}$ being the T_0-time price volatility function for maturity T_j.

Appendix B. ST18 model conditional on variance path

Let $W_t^{F_j} = \rho_{FV}W_t^V + \sqrt{1-\rho_{FV}^2}X_t$, where W^V and X are independent standard Brownian motions. We then obtain for the log-futures price in the ST18 model,

$$df\left(t,T_j\right) = -\frac{1}{2}\alpha_j^2e^{-2\gamma(T_j-t)}V_tdt + \alpha_j\rho_{FV}e^{-\gamma_j(T_j-t)}\sqrt{V_t}dW_t^V + \alpha_j\sqrt{1-\rho_{FV}^2}e^{-\gamma_j(T_j-t)}\sqrt{V_t}dX_t. \tag{B.1}$$

In addition,

$$dV_t = \kappa\left(\theta - V_t\right)dt + \sigma_V\sqrt{V_t}dW_t^V,$$

from which it follows that

$$\begin{aligned} \sqrt{V_t}dW_t^V &= \frac{dV_t - \kappa\left(\theta - V_t\right)dt}{\sigma_V},\\ e^{-\gamma_j(T_j-t)}\sqrt{V_t}dW_t^V &= \frac{e^{-\gamma_j(T_j-t)}}{\sigma_V}dV_t - \frac{\kappa\theta}{\sigma_V}e^{-\gamma_j(T_j-t)}dt + \frac{\kappa}{\sigma_V}e^{-\gamma_j(T_j-t)}V_tdt. \end{aligned} \tag{B.2}$$

Furthermore,

$$\begin{aligned} d\left(e^{\gamma_jt}V_t\right) &= \gamma_je^{\gamma_jt}V_tdt + e^{\gamma_jt}dV_t \Rightarrow\\ e^{\gamma_jT_0}V_{T_0} &= e^{\gamma_jt}V_t + \gamma_j\int_t^{T_0}e^{\gamma_js}V_sds + \int_t^{T_0}e^{\gamma_js}dV_s \Rightarrow\\ \int_t^{T_0}e^{\gamma_js}dV_s &= e^{\gamma_jT_0}V_{T_0} - e^{\gamma_jt}V_t - \gamma_j\int_t^{T_0}e^{\gamma_js}V_sds. \end{aligned} \tag{B.3}$$

Substituting (B.3) into (B.2) and integrating, we obtain

$$\begin{aligned} \int_t^{T_0}e^{-\gamma_j(T_j-s)}\sqrt{V_s}dW_s^V &= \frac{e^{-\gamma_jT_j}}{\sigma_V}\int_t^{T_0}e^{\gamma_js}dV_s - \frac{\kappa\theta}{\sigma_V}e^{-\gamma_jT_j}\int_t^{T_0}e^{\gamma_js}ds + \frac{\kappa}{\sigma_V}e^{-\gamma_jT_j}\int_t^{T_0}e^{\gamma_js}V_sds\\ &= \frac{e^{-\gamma_jT_j}}{\sigma_V}\left(e^{\gamma_jT_0}V_{T_0} - e^{\gamma_jt}V_t\right) - \frac{\gamma_je^{-\gamma_jT_j}}{\sigma_V}\int_t^{T_0}e^{\gamma_js}V_sds - \frac{\kappa\theta}{\sigma_V\gamma_j}e^{-\gamma_jT_j}\left(e^{\gamma_jT_0} - e^{\gamma_jt}\right) + \frac{\kappa e^{-\gamma_jT_j}}{\sigma_V}\int_t^{T_0}e^{\gamma_js}V_sds. \end{aligned}$$

[7] $b_0(t,T_1,T_2)$ and $b_1(t,T_1,T_2)$ are functions of time, but we refer to them simply as b_0 and b_1.

[8] These expressions are obtained following the indications in Frau and Fanelli (2024, Sec. B.2) (this work provides an alternative framework consistent with the 2-terms CF schedule we propose in this work).

[9] $c_{1,j}(T_0,T_j)$ and $d_{2,j}(T_0,T_j)$ are functions of time, but we refer to them simply as $c_{1,j}$ and $d_{2,j}$.

Returning to (B.1), we obtain

$$\begin{aligned}
f\left(T_0,T_j\right) &= f\left(t,T_j\right) - \frac{1}{2}\alpha_j^2 e^{-2\gamma_j T_j}\int_t^{T_0} e^{2\gamma_j s}V_s\,ds + \alpha_j\rho_{FV}e^{-\gamma_j T_j}\int_t^{T_0} e^{\gamma_j s}\sqrt{V_s}\,dW_s^V + \alpha_j\sqrt{1-\rho_{FV}^2}e^{-\gamma_j T_j}\int_t^{T_0} e^{\gamma_j s}\sqrt{V_s}\,dX_s \\
&= f\left(t,T_j\right) - \frac{1}{2}\alpha_j^2 e^{-2\gamma_j T_j}\int_t^{T_0} e^{2\gamma_j s}V_s\,ds + \alpha_j\rho_{FV}\left[\frac{e^{-\gamma_j T_j}}{\sigma_V}\left(e^{\gamma_j T_0}V_{T_0} - e^{\gamma_j t}V_t\right) - \frac{\gamma_j e^{-\gamma_j T_j}}{\sigma_V}\int_t^{T_0} e^{\gamma_j s}V_s\,ds\right. \\
&\quad \left. - \frac{\kappa\theta}{\sigma_V\gamma_j}e^{-\gamma_j T_j}\left(e^{\gamma_j T_0} - e^{\gamma_j t}\right) + \frac{\kappa e^{-\gamma_j T_j}}{\sigma_V}\int_t^{T_0} e^{\gamma_j s}V_s\,ds\right] + \alpha_j\sqrt{1-\rho_{FV}^2}e^{-\gamma_j T_j}\int_t^{T_0} e^{\gamma_j s}\sqrt{V_s}\,dX_s \\
&= f\left(t,T_j\right) - \frac{\alpha_j\rho_{FV}\kappa\theta}{\sigma_V\gamma_j}e^{-\gamma_j T_j}\left(e^{\gamma_j T_0} - e^{\gamma_j t}\right) + \frac{\alpha_j\rho_{FV}}{\sigma_V}e^{-\gamma_j T_j}\left(e^{\gamma_j T_0}V_{T_0} - e^{\gamma_j t}V_t\right) \\
&\quad - \frac{1}{2}\alpha_j^2\int_t^{T_0}\left(e^{-2\gamma_j(T_j-s)} - \frac{2\rho_{FV}\kappa}{\alpha_j\sigma}e^{-\gamma(T_j-s)} + \frac{2\rho_{FV}\gamma_j}{\alpha_j\sigma_V}e^{-\gamma(T_j-s)}\right)V_s\,ds + \alpha_j\sqrt{1-\rho_{FV}^2}e^{-\gamma_j T_j}\int_t^{T_0} e^{\gamma_j s}\sqrt{V_s}\,dX_s.
\end{aligned}$$

Conditional on the variance path, we finally get that $f\left(T_0,T_j\right)$ has a normal distribution with mean

$$f\left(t,T_j\right) - \frac{\alpha_j\rho_{FV}\kappa\theta}{\sigma_V\gamma_j}e^{-\gamma_j T_j}\left(e^{\gamma_j T_0} - e^{\gamma_j t}\right) + \frac{\alpha_j\rho_{FV}}{\sigma_V}e^{-\gamma_j T_j}\left(e^{\gamma_j T_0}V_{T_0} - e^{\gamma_j t}V_t\right) - \frac{1}{2}\alpha_j^2\int_t^{T_0}\left(e^{-2\gamma_j(T_j-s)} - \frac{2\rho_{FV}\kappa}{\alpha_j\sigma_V}e^{-\gamma(T_j-s)} + \frac{2\rho_{FV}\gamma_j}{\alpha_j\sigma_V}e^{-\gamma(T_j-s)}\right)V_s\,ds,$$

and variance

$$\alpha_j^2\left(1-\rho_{FV}^2\right)e^{-2\gamma_j T_j}\int_t^{T_0} e^{2\gamma_j s}V_s\,ds.$$

Appendix C. Supplementary data

Online supplementary material is available at https://doi.org/10.1016/j.eneco.2025.108809.

References

Alfeus, M., Schloegl, E., 2019. On spread option pricing using two-dimensional Fourier transform. Int. J. Theor. Appl. Finance 22 (5).
Andersen, L., 2008. Simple and efficient simulation of the Heston stochastic volatility model. J. Comput. Finance 11 (3), 1–42.
Bates, D.S., 1996. Jumps and stochastic volatility: Exchange rate processes implicit in Deutsche Mark options. Rev. Financ. Stud. 9 (1), 69–107.
Bjerksund, P., Stlensland, G., 2014. Closed form spread option valuation. Quant. Finance 14 (10), 1785–1794.
Black, F., 1976. The pricing of commodity contracts. J. Financ. Econ. 3 (1), 167–179.
Black, F., Scholes, M., 1973. The pricing of options and corporate liabilities. J. Political Econ. 81 (3), 637–654.
Caldana, R., Fusai, G., 2013. A general closed-form spread option pricing formula. J. Bank. Financ. 37 (12), 4893–4906.
Cont, R., Tankov, P., 2004. Financial Modelling with Jump Processes. Chapman and Hall/CRC Financial Mathematics Series.
Crosby, J., Frau, C., 2022. Jumps in commodity prices: New approaches for pricing plain vanilla options. Energy Econ. 14, 106302.
D'Ecclesia, R.L., Magrini, E., Montalbano, P., Triulzi, U., 2014. Understanding recent oil price dynamics: A novel empirical approach. Energy Econ. 46, S11–S17.
Dempster, M.A.H., Hong, S.S.G., 2002. Spread option valuation and the fast Fourier transform. In: Geman, H., Madan, D., Pliska, S.R., Vorst, T. (Eds.), Mathematical Finance – Bachelier Congress 2000: Selected Papers from the First World Congress of the Bachelier Finance Society. Paris, June 29 to July 1, 2000, Springer Berlin Heidelberg, pp. 203–220.
Fang, F., Oosterlee, C.W., 2008. A novel pricing method for European options based on Fourier-cosine series expansions. SIAM J. Sci. Comput. 31 (2), 826–848.
Frau, C., Fanelli, V., 2024. Seasonality in commodity prices: New approaches for pricing plain vanilla options. Ann. Oper. Res. 336 (1), 1089–1131.
Heston, S.L., 1993. A closed-form solution for options with stochastic volatility with applications to bond and currency options. Rev. Financ. Stud. 6 (2), 327–343.
Hurd, T., Zhou, Z., 2010. A Fourier transform method for spread option pricing. SIAM J. Financ. Math. 1, 142–157.
Kirk, E., 1995. Correlation in the energy markets, managing energy price risk. Risk Books 1, 71–78.
Kyriakou, I., Brignone, R., Fusai, G., 2024. Unified moment-based modeling of integrated stochastic processes. Oper. Res. 72 (4), 1630–1653.
Kyriakou, I., Nomikos, N.K., Papapostolou, N.C., Pouliasis, P.K., 2016a. Affine-structure models and the pricing of energy commodity derivatives. Eur. Financ. Manag. 22 (5), 853–881.
Kyriakou, I., Pouliasis, P.K., Papapostolou, N.C., 2016b. Jumps and stochastic volatility in crude oil prices and advances in average option pricing. Quant. Finance 16 (12), 1859–1873.
Margrabe, W., 1978. The value of an option to exchange one asset for another. J. Financ. 33, 177–186.
Merton, R., 1976. Option pricing when underlying stock returns are discontinuous. J. Financ. Econ. 3 (1–2), 125–144.
Ravindran, K., 1993. Low-fat spreads. Risk 6 (10), 56–57.
Schneider, L., Tavin, B., 2018. From the Samuelson volatility effect to a Samuelson correlation effect: an analysis of crude oil calendar spread options. J. Bank. Financ. 95, 185–202.
Trolle, A.B., Schwartz, E.S., 2009. Unspanned stochastic volatility and the pricing of commodity derivatives. Rev. Financ. Stud. 22 (11), 4423–4461.
Venkatramanan, A., Alexander, C., 2011. Closed form approximations for spread options. Appl. Math. Finance 18 (5), 447–472.